ESA BASED FIBER OPTICAL HUMIDITY SENSOR

by
Qiao Chen

This thesis has been submitted to the faculty of
Virginia Polytechnic Institute and State University
in partial fulfillment of the requirements for the degree of
Master of Science
in
Electrical Engineering

Dr. Richard Claus, Chairman

Dr. William Spillman

Dr. Ira Jacobs

Nov 21, 2002
Blacksburg, VA

Key words: Self-Assembly, Optical Fiber Sensor, Relative Humidity, Fabry-Perot Interferometer, Nanotechnology

ESA-BASED FIBER OPTICAL HUMIDITY SENSOR

by
Qiao Chen

Committee Chair: Richard O.Claus

ECE Dept, VTech

(ABSTRACT)

Several techniques for measuring humidity are presented. The goal of the study is to use the electrostatic self-assembled monolayer synthesis process to fabricate a Fabry-Parot Cavity based optical fiber humidity sensor. The sensing scheme bases on the refractive index change with relative humidity of the film applied to the end of optical fiber. That is, the change in reflected optical power indicates certain humidity. To achieve this, some chemicals induce on specific coating materials were applied at the end of optical fiber. In this thesis, experimental results are given to prove that the humidity sensor has high sensitive and fast response time. Furthermore, we investigate the potential for the use of human breathing monitoring and air flow rate detection. Results from preliminary tests of each are given.

Acknowledgments

I would like to express my gratitude to my advisor, and committee chair:Dr. R.O.Claus. Without his encouragement and guidance I would never have made it here. I would also like to thank Dr. William Spillman and Dr. Ira Jacobs for taking the time to serve on my committee and for contributing to my professional development. It has been both an honor and a privilege.

I would like to acknowledge many meaningful discussions with colleagues Dr. Tingying Zheng, Dr. You-Xiong Wang, Dr. Liangmin Zhang, Dr. Ken Meissner, Dr. F.J Arregui, and Fajian Zhang that have greatly contributed to both my research and the final form of this thesis. In addition, thanks to all of the FEORC researchers and support staff for your encouragement and assistance.

At last, a sincere thanks is extended to my parents, without whose help I would never have been able to receive a Bachelors Degree. Thanks.

TABLE OF CONTENTS

TABLE OF FIGURES

LISTS OF TABLES

Chapter I Introduction

1.1 Optical Fiber Sensors

Due to the intrinsic characteristics of fiber optics, the advantages listed below [1] make them attractive for a multitude of sensing applications. It has been nearly forty years since the appearance of the first optical fiber sensor. Fiber sensors still retain their fascination for scientists and technologists.

- Nonelectrical
- Explosion-proof
- Often do not require contact
- Remotable
- Small size and weight
- Allow access into normally inaccessible areas
- Potentially easy-to-install
- Immune to radio frequency interference and electro-magnetic interference
- Solid-state reliability
- High accuracy
- Can be interfaced with data communication systems
- Secure data transmission
- Potentially resistant to ionizing radiation

Basically, fiber-optic sensors can be divided into two types: extrinsic sensors (Fig 1.1), which use the glass fiber for conveying information collected by another device, and intrinsic sensors (Fig 1.2), which make measurements by detecting perturbations in the light carried in the fiber. All fiber-optic sensors are undoubtedly impervious to electromagnetic fields and such advantages are not available from any conventional wired devices. This offers numerous applications in the electrical power industry. On the other hand, fiber-optic sensors are widely used in the case of conductive fluids such as blood

and seawater. The attraction in medical and biomedical fiber-optic sensors is the avoidance of the need to take away samples for remote chemical analysis. [2]

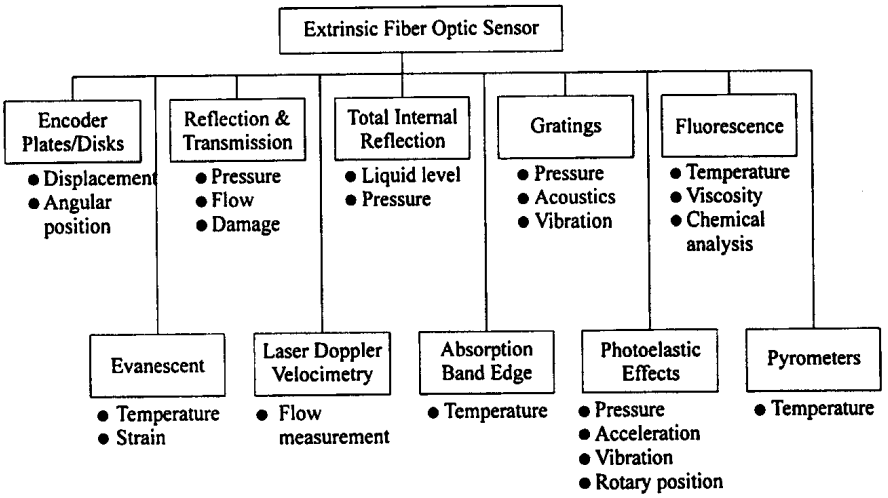

Figure 1.1 Extrinsic fiber optic sensor applications.

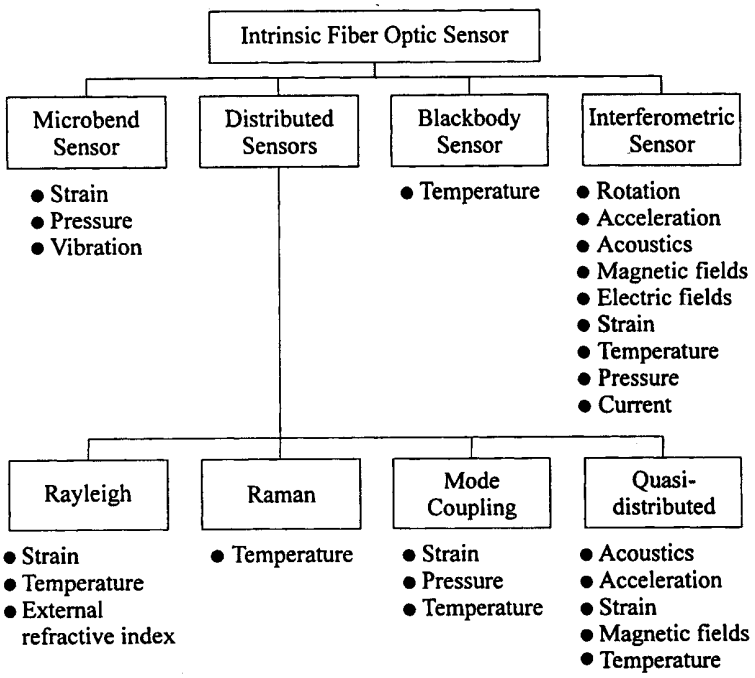

Figure 1.2 Intrinsic fiber optic sensor applications. [3]

In addition, the intrinsic characteristics of optical fiber such as explosion-proof operation and immunity to temperature and pressure make them a suitable candidate in chemical and smart structures monitoring applications. A widely used application is as fiber-optic strain gauges. Structural engineers embed them in concrete in order to monitor bridge deflections under traffic loads, and aeronautical engineers use them to monitor the deformation of aircraft components[2].

So far, fiber sensors have gained a significant commercial foothold, primarily in fiber gyroscopes, pressure and temperature sensors[2]. A recent Frost & Sullivan study estimated that the market for fiber-optic pressure sensors alone will increase to $22 million by 2006[3].

It is clear that fiber optics will play an important role in sensing technology in the future. According to a report submitted by the International Technology Research Institute at Loyola University, the international market for fiber-optic sensors could be as high as $5 billion by 2010[3].

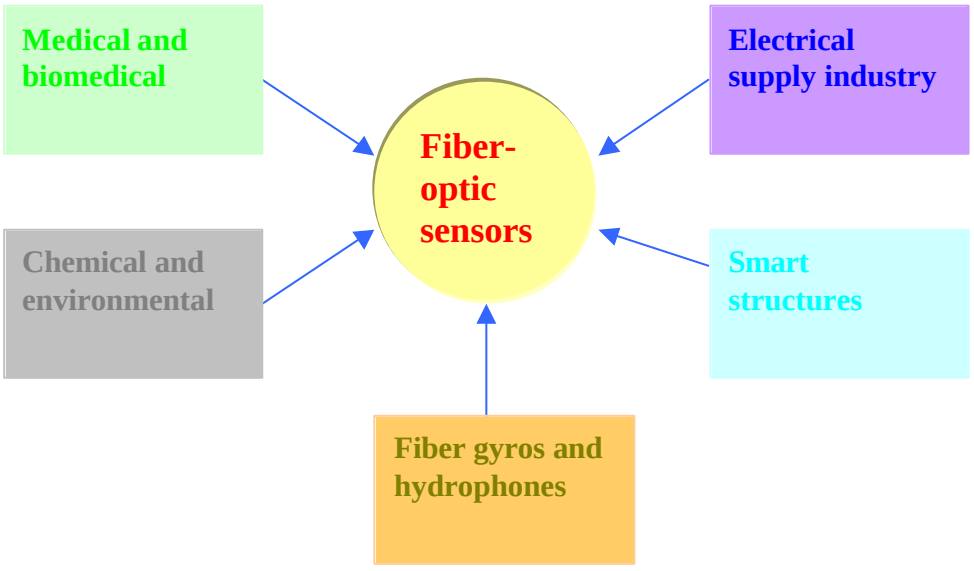

Figure 1.3 Established application sectors for fiber-optic sensors.[2]

1.2 Optical fiber humidity sensors

a. Basic concepts of humidity

1. The water content in the surrounding air is an important factor for the well-being of humans and animals. Here, the amount of water vapor in the air is described by the term "humidity." As humidity is a very common, continuously changing component of our environment, the measurement and/or the control of humidity are important not only for human comfort, but also for a broad spectrum of application fields, such as automotive electronics, medical service, fine mechanisms, and meteorology.[5] Relative humidity and absolute humidity are two common terms connected with humidity measurement technology and are defined as follows.

Absolute humidity: The mass of water vapor in a given volume of air (i.e. density of water vapor in a given volume, usually expressed in grams per cubic meter). Since this measure is also a function of atmospheric pressure, it is not generally useful in engineering practice.

Relative humidity (RH): The amount of water vapor actually in the air divided by the amount of water vapor the air can hold. As a percentage expression, RH is defined as

$$H = 100\frac{P_w}{P_s},$$

where P_w is the partial pressure of water vapor and P_s is the pressure of saturated water vapor at a given temperature.

(Note that in this thesis, whenever humidity is mentioned, relative humidity is assumed.)

b. Humidity sensors

The measurement of relative humidity has always been a difficult issue because of the interaction of other variables such as temperature and gas in the air[7-9]. There are many ways to detect humidity. Generally, humidity sensors can be divided into three major groups: those that measure mechanical property changes; psychrometric measurements that compare the latent heat of evaporation of a saturated environment to the environment;

and those that respond to electrical or optical property change such as resistance, capacitance, and color.

Although various materials are used in humidity sensors, polymer film based sensors have attracted a great deal of interest in recent years. Many different types have been developed, which can be categorized as follows. [5]

- Capacitance types
- Resistance types, including ionic and electronic conduction versions
- Transistor structures (FET, CFT)
- Resonators
- Electrochemical types
- Fiber-optic types

According to many reports, small and low cost polymer thin film sensors have been fabricated for integrated microsensors, and response times of such commercial available humidity sensors are on the order of seconds. In this thesis, only polymer-based fiber optic sensors have been analyzed.

c. Polymer based optical fiber humidity sensors[6]

There are many interactions that can modulate the properties of the light transmitted in an optical fiber by causing phase, intensity, polarization, or spectral changes.Generally speaking, the basic idea is to use polymer to form part of optical path to modulate either the reflective index or the coefficient of absorbance. Respectively, there are also various different sensor structures, which are divided as follows.

- Optrode-Style Sensors (Fig. 1.4)
- Core-Based Sensors (Fig. 1.5)
- Coating-Based Sensors (Fig. 1.6)
- Interferometric Sensors (Fig. 1.7)

Similarly to the structure shown in Figure 1.4, in this thesis, applying new nano-technology-electrostatic self assembly (ESA) methods, a polymer based optical fiber humidity sensor has been fabricated with a nano-structured Fabry-Perot interferometer

formed at the end of the fiber. More details concerning sensor design and synthesis will be reviewed in the following chapters, and promising results about humidity detection will be given.

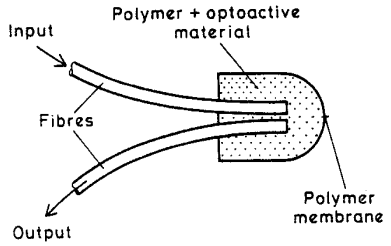

Figure 1.4 Schematic structure of the optrode-style fiber-optic sensors.[6,12]

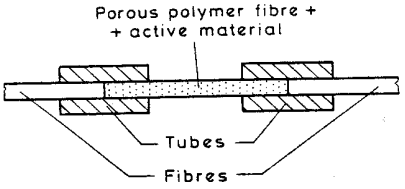

Figure 1.5 Typical core-based sensor using porous polymer core.[6]

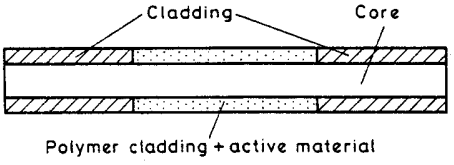

Figure 1.6 Fiber-optic sensor with sensitive cladding.[6,10]

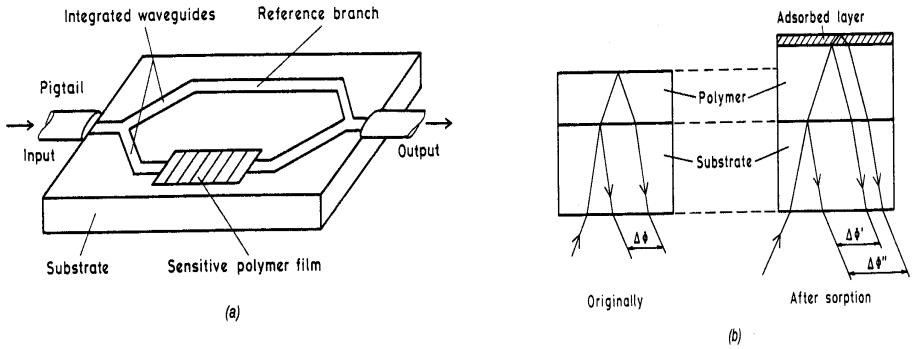

Figure 1.7 Interferometric sensors: (a) transmission type; (b) reflection type.[6,11]

1.3 Thesis Objective and Overview

The primary objective of this thesis is to describe the fabrication and evaluation of an ESA-based optical fiber humidity sensor. This specifically includes the following sub-topics.

- Design and fabrication of an optical fiber-based self-assembled thin film humidity sensor

- Evaluation of quantitative sensor performance using calibrated relative humidity standards

- Design, fabrication and testing of initial low-cost electronic and optoelectronic breadboard circuits to support the humidity sensor instrumentation

- Measurement of the rise time of the humidity sensor

- Use of two humidity sensors to quantify airflow dynamics

This thesis is organized as follows. Chapter 2 presents a discussion of principles behind the fiber-optic humidity sensor, including an introduction concerning basic interference and Fabry-Perot interferometry. The ESA process and the fabrication of the fiber-optic humidity sensor are discussed in Chapter 3. Chapter 4 summarizes details about system setup and sensor fabrication. In Chapter 5, test results of humidity sensors are given. Taking advantage of the ESA method, the sensor exhibits a fast response time and is able to quantify human breathing and airflow rate. The thesis concludes with a summary of the significance and primary contributions of this investigation. Finally, recommendations for future research work are suggested in Chapter 6.

Chapter II Basic operation of sensor

2.1 Introduction

The sensing mechanism of this fiber-optic humidity sensor relies on the change in the reflected optical power that is induced by water molecules on specific polymer coatings, forming variable interferometric cavities at the end of the fiber. This chapter reviews the basic principle of nano-structured Fabry-Perot interferometers and thin film interference filters. Through this analysis, the principle of our humidity sensor is explained.

2.2 Nano-structured fiber Fabry-Perot interferometer (FPPI)[13,14]

As is well known, a classic fiber Fabry-Perot interferometer (FFPI) consists of two mirrors separated by a distance L in an optical fiber[13,14]. These mirrors have a reflectance and transmittance of R_i and T_i, respectively. Assuming the absorbance of the mirrors and other losses are A_i, energy conservation is satisfied if $A_i+R_i+T_i=1$ for i^{th} mirror (i=1,2).

When light amplitude I is incident on the i^{th} Fabry-Perot mirror, the reflected light and the transmitted light can be written as $jI\sqrt{R_i}$ and $I\sqrt{T_i}$, respectively.

The ratio of the reflected amplitude to the incident amplitude, $r_{FP,}$ can be defined as

$$r_{FP} = j\sqrt{R_1} + j\sqrt{R_2}T_1e^{jf} - j\sqrt{R_2}T_1\sqrt{R_1R_2}e^{2jf} + j\sqrt{R_2}T_1R_1R_2e^{3jf} + \cdots$$

$$= j\sqrt{R_1} + j\sqrt{R_2}T_1e^{jf}\sum_0^\infty s^n ,$$

where $s = -\sqrt{R_1R_2}e^{jf}$, and the phase shift of interferometer is $f = \frac{4pnL}{l}$.

$$|s| << 1$$

$$\sum_0^\infty s^n = \frac{1}{1-s} \qquad \textbf{(2-1)}$$

$$R_{FP} = |r_{FP}|^2 = \frac{R_1 + R_2(1-A_1)^2 + 2\sqrt{R_1R_2}(1-A_1)\cos f}{1+R_1R_2 + 2\sqrt{R_1R_2}\cos f}$$

Similarly, the ratio of transmitted to incident amplitude t_{FP} can be written as

$$t_{FP} = \sqrt{T_1T_2} - \sqrt{R_1R_2T_1T_2}e^{jf} + R_1R_2\sqrt{T_1T_2}e^{2jf} + \cdots$$

$$= \sqrt{T_1 T_2} \sum_0^\infty s^n ,$$

So $$T_{FP} = |t_{FP}|^2 = \frac{T_1 T_2}{1 + R_1 R_2 + 2\sqrt{R_1 R_2}\cos f} . \qquad \textbf{(2-2)}$$

From this analysis, it is obvious that there are three main characteristics: R_1, R_2 and L, that can greatly influence the ratio R_{FP}. While different from the traditional FPPI that relies on a variation in the length L, the new philosophy of the nano-structured FPPI is to change R_2, the reflection of the external mirror at the end face of the optical fiber. Figure 2.1 shows a simulation result of reflectivity R from such a structure corresponding to changing R2 from 0.3 to 0.9. It can be seen that R has same characteristic except different values under same scales. Furthermore, by varying the reflect index of R2, the reflect intensity of the FP cavity is suppose to have a variation. And the change of R2 are due to the change of relative humidty

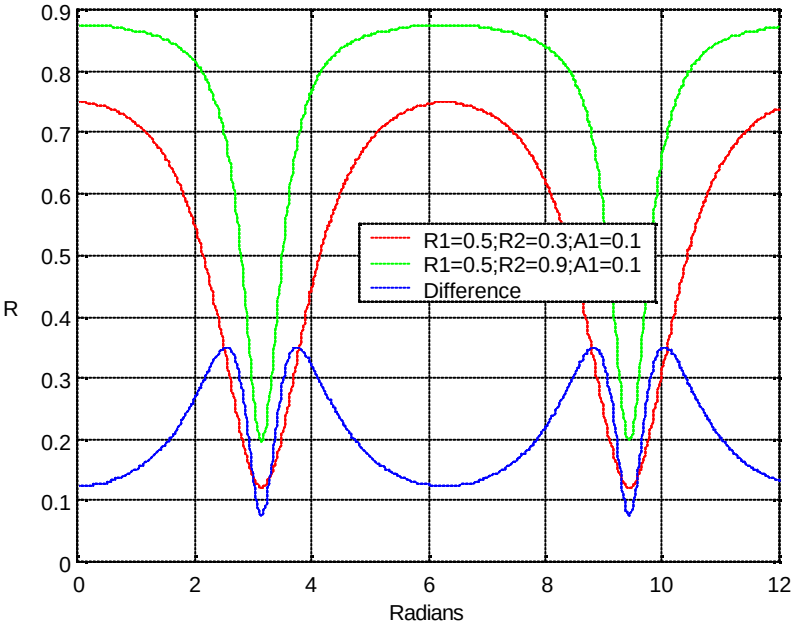

Figure 2.1 Reflectance of a nano-structured Fabry-Perot interferometer with R_1=0.5 when R_2 changes from 0.3 to 0.9. (Assuming mirrors are lossless).[15]

2.3 The interference filter on the end of the fiber

In our design, an effective thin film interference filter is coated on the end of the fiber to change the reflection, R_2. With the help of TFCalc software, the interference filter may be designed and optimized (TFCalc, Software Spectra Inc, version 3.4.3, 1998). To understand the interference filter better, it is necessary to discuss some basic concepts employed in such filters.

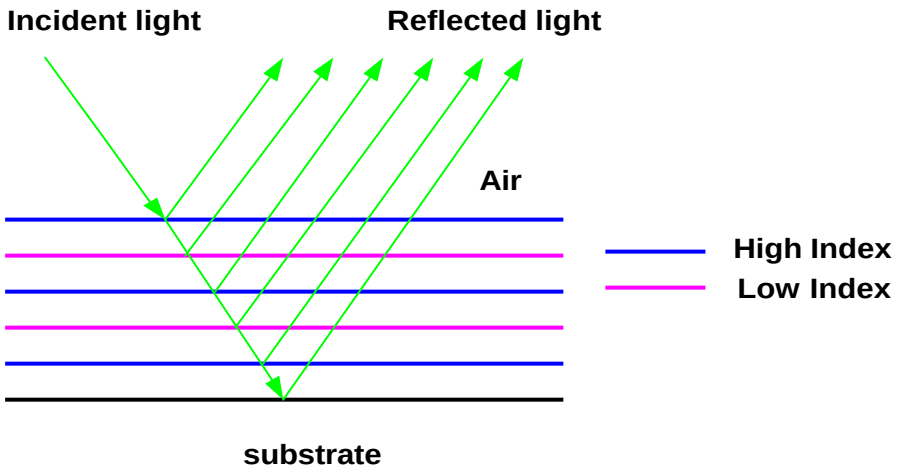

Figure 2.2 Reflection and transmission at layer boundaries.[16]

First, refering to Figure 2.2, and, assuming r is the ratio of the refractive indices at a boundary between two media, the amplitude of the reflected light at the boundary can be written

$$R = \frac{1-r}{1+r} \,. \qquad (2\text{-}3)$$

Second, there is a π phase shift at the turning point that is strictly valid for lossless media. Third, incident light, which is reflected from both the top and bottom surfaces of a thin

film such as that shown in Figure 2.3, will recombine constructively or destructively, depending on whether the differential phase shift is 2nπ or (2n+1) π.

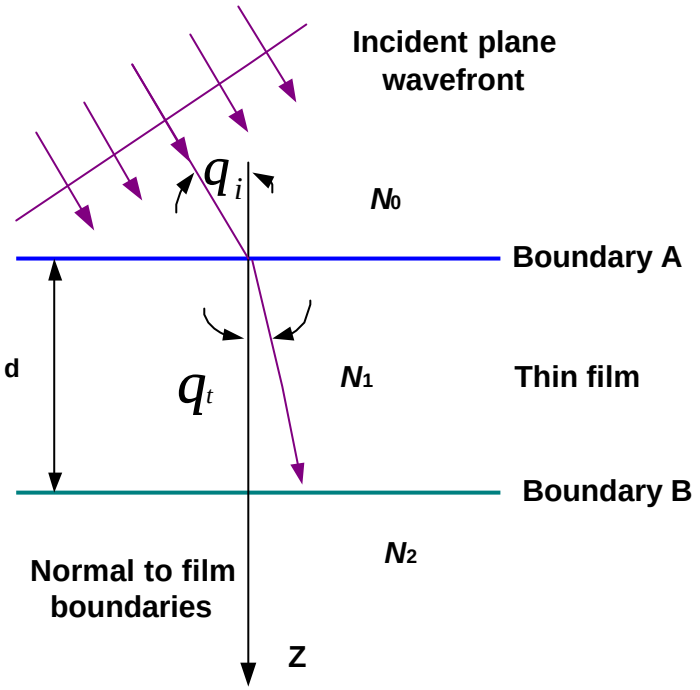

Figure 2.3 Plane wave incident on a thin film.[16]

Now, consider a quarter wavelength thickness thin film. For such a structure, the construction of interference from reflections at both surfaces can be easily achieved. Associated reflection and transmission ratios at the interfaces are dependent upon incidence angle and are given by Fresnel equations [14]. For s polarization (TE for transverse electric)

$$r_s = \frac{n_i \cos q_i - n_t \cos q_t}{n_i \cos q_i + n_t \cos q_t} \text{ and } t_s = \frac{2n_i \cos q_i}{n_i \cos q_i + n_t \cos q_t}. \qquad \textbf{(2-4)}$$

For p polarization (TM for transverse magnetic)

$$r_p = \frac{n_t \cos q_i - n_i \cos q_t}{n_i \cos q_t + n_t \cos q_i} \text{ and } t_p = \frac{2n_i \cos q_i}{n_i \cos q_t + n_t \cos q_i}, \quad \textbf{(2-5)}$$

where θ_I and θ_t are the angles made by the incident and transmitted light with the surface normal at the boundary between the incident and transmitted media, respectively.

This effect can be enhanced by reflection from multiple layers since the light reflected from all interfaces within the quarter wavelength stack film have equal phase when they reach the top surface of the film. What is required here is a stack of alternating high and low index quarter wavelength films. Additionally, the first layer, next to the substrate and the outermost layer must be high-index films.

When plane polarized light passes through thin films, the relationship between the electrical field E and magnetic field H is given as

$$\begin{bmatrix} E_I \\ H_I \end{bmatrix} = M \begin{bmatrix} E' \\ H' \end{bmatrix} = M_1 M_2 \cdots M_m \begin{bmatrix} E' \\ H' \end{bmatrix}, \quad \textbf{(2-6)}$$

where M_m is the characteristic matrix of the m^{th} layer, and can be written as:

$$M_m = \begin{bmatrix} \cos f_m & \frac{i \sin f_m}{n_m} \\ i n_m \sin f_m & \cos f_m \end{bmatrix}. \quad \textbf{(2-7)}$$

In the matrix elements, f_m is the phase shift introduced by d_m, the thickness of the m^{th} layer, so

$$f_m = \frac{2p}{l} n_{ml} d_m \cos a, \quad \textbf{(2-8)}$$

where a is the incidence angle of the light, l is the wavelength, and n_{ml} follows the convention

$$n_{ml} = n_{ms} = n \cos a \text{, for s or perpendicular polarization,} \quad \textbf{(2-9)}$$

$$n_{ml} = n_{mp} = \frac{n_m}{\cos a}, \text{ for p or parallel polariztion, and} \quad \textbf{(2-10)}$$

$$n_{ml} = n_m, \text{ for normal incidence,} \quad \textbf{(2-11)}$$

where n_m is the refractive index of the material of a single layer m[16,17].

Based on the analysis above, the expression for reflectance R of such multilayer thin films becomes

$$R_{l/4} = \left(\frac{1 - \left(n_H / n_L \right)^{2p} \left(n_H^2 / n_s \right)}{1 + \left(n_H / n_L \right)^{2p} \left(n_H^2 / n_s \right)} \right)^2, \quad \textbf{(2-12)}$$

where p is the number of layers. Given the layer numbers p, the reflectance R can be increased if the ratio n_H/n_L becomes large. Once given the index ratio between two layers, R can be adjusted by the number of layers p. Figure 2.4 illustrates the change in spectral characteristics for such a dielectric stack with an increasing number of quarter wavelength layers. The figure here shows that the magnitude of peak reflectance as well as the number of sideband oscillations increases with an increasing number of λ/4 layers. Also, the spectral width of the reflectance peak is dependent upon the ratio of the refractive indices of the high and low index layers.

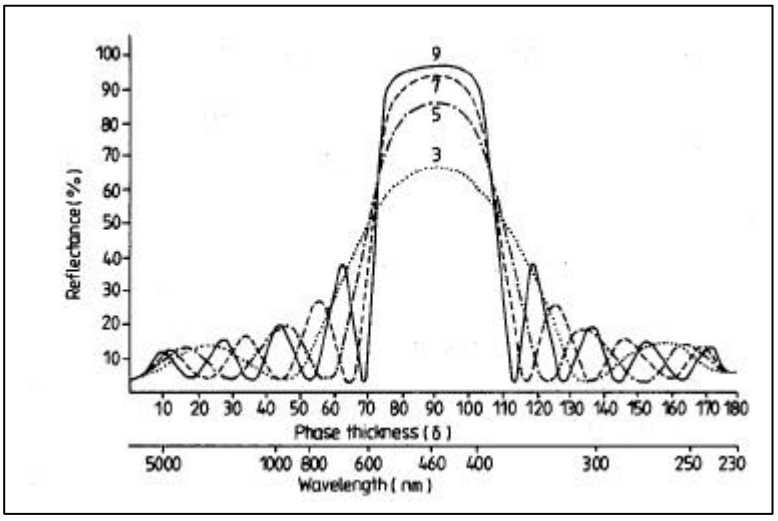

Figure 2.4 Theoretical reflectance spectra of multilayer stacks formed of alternating l/4 layers of n_H=2.3 and n_L=1.38 on glass (n_s=1.52) as a function of phase thickness (2pnd/l). The number of layers is indicated.[18]

2.4 Principles of ESA based optical fiber sensor

Figure 2.5 shows the structure of our nano-structured Fabry-Perot optical fiber sensor, where the coating functions as a mirror. Applying Fresnel's law, and assuming normal incidence conditions, the reflectance of the two mirrors are

$$R_1 = \frac{(n_1 - n_2)^2}{(n_1 + n_2)^2} \text{ and } \quad R_2 = \frac{(n_2 - n_3)^2}{(n_2 + n_3)^2}, \tag{2-13}$$

where R_1 is the reflection coefficient at the first interface (optical fiber-coating) and R_2 is the reflection coefficient at the second interface (coating-air).

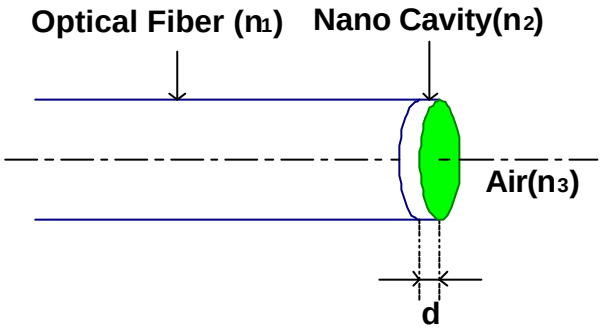

Figure 2.5 Thin film interferometric cavity. [19,20]

Rewriting Equation 2-1, the ratio between the reflected optical power and the incident optical power is then

$$R_{FP} = \frac{R_1 + R_2(1-A_1)^2 \exp(-4ad) - 2\sqrt{R_1 R_2}(1-A_1)\exp(-2ad)\cos f}{1 + R_1 R_2 \exp(-4ad) - 2\sqrt{R_1 R_2}\exp(-2ad)\cos f} \text{ [19]}, \tag{2-14}$$

where a is the optical absorption coefficient and d is the coating thickness.

As mentioned in the first section, a classic FPPI works by using the variation of d to produce a phase shift, and thus, a change in intensity of reflected optical power. Since the

sensor proposed in this thesis has been proved a fast response time, which is on the order of microseconds, the thickness d here can be treated as unchanged during the sensing period. Therefore, the new philosophy of this new Fabry-Perot etalon is to change this intensity by varying the reflection of the external mirror at the endface of the optical fiber, R_2. Because the coating material is hydrophilic, microscopic water drops can change the interface between the coating and the air—R_2. Employing the simulation result from Fig. 2.1, we thus expect to see a variation in reflected power when different numbers of water molecules are applied to our optical fiber humidity sensor. Also, in this nano-structured Fabry-Perot sensor, we can use ESA process to optimize the thickness d, and refractive index of the thin film filter on the tip of the optical fiber. Therefore, this will optimize the output of our humidity sensors. In the next two chapters, the hypothesis introduced in this section will be analyzed, more details about the ESA process will be presented and sensor fabrication will be summarized. In Chapter V, the results using both single mode fiber (SMF) and multimode fiber (MMF) are given. The principle behind the SMF is illustrated in this chapter. For MMF, the humidity will also change the reflective index of thin film coating at the end of the fiber, but the principle is no longer interference. While, both sensing schemes will induce reflect optic power change.

Chapter III ESA

3.1 Introduction

Electrostatic Self Assembly (ESA) is a fabrication process to deposit coatings on glass, silicon, polymer and metallic substrates. The basic principle behind ESA is the alternate adsorption of oppositely charged polyions on a charged substrate. In past research work, a number of fabrication methods have been developed to form multilayer nanostructured thin films. Among these methods, the most commonly used processes are Langmuir-Blodgett (L-B) self-assembly methods and chemical self-assembled monolayer (SAM) methods. Unfortunately, LB films are expensive and not sufficiently robust for many applications due to the occurrence of defects. SAMs are also difficult to apply for multilayer film fabrication because of the very high-yield chemical reactions required by the film fabrication process[21]. Unlike the LB and SAM schemes, ESA processing offers a number of advantages that make it widely adapted for the incorporation of molecules, including nonlinear optical chromophores, conducting polymers, biological marcromolecules, magnetic materials, dielectrics, and metallic or metallic oxide nanoparticles. Due to the intrinsic characters of ESA thin films, such as cost and ease of fabrication, these thin films are suitable for a variety of applications, including optics, electronics, biosensors, humidity sensors and linear and nonlinear optical thin films[22-25]. In this chapter, the basic model for multilayer thin film fabrication will be introduced and testing results will be given about the characteristics of ESA thin films.

3.2 ESA process technology

ESA thin films can be coated on different substrates such as quartz, glass and single crystal silicon, yet before the fabrication, the substrates are required to be pre-charged and cleaned. For glass substrates such as the glass in optical fibers, the processing steps involve two sub-processes:

1. Clean the substrate with piranha solution: a 30:70 mixture of hydrogen peroxide (H_2O_2) and concentrated sulfuric acid (H_2SO_4) at room temperature, and
2. Clean the resulting negatively charged substrate with ultra-pure water and drying it in an oven. This process is called 'functionlizing' the substrate.[26]

Figure 3.1 shows basic concepts behind the ESA process. On the left, a negatively charged substrate 'functionalized' as described above is immersed into a water solution, which contains cationic molecules with fixed positive functional groups. The cationic molecules are attracted by the anionic substrate and automatically rearrange themselves to form a molecular monolayer.

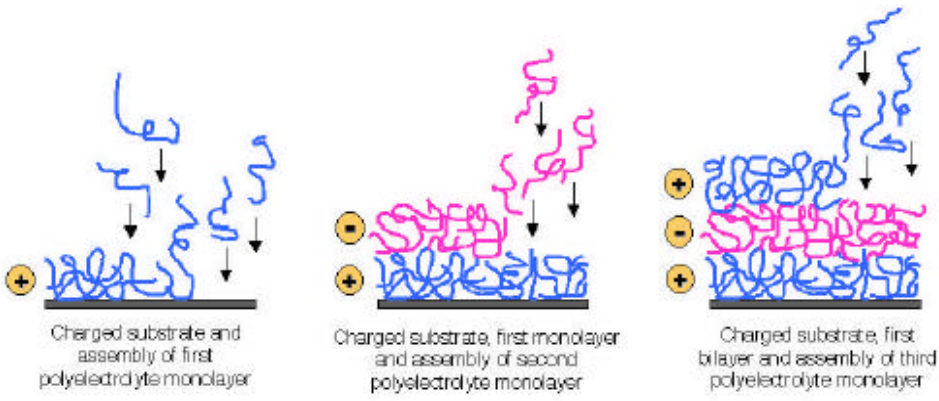

Figure 3.1 ESA Schematic for Buildup of Multi-Layer Assemblies by Consecutive Adsorption of Anionic and Cationic Molecule-Based Polyelectrolytes.

After rinsing with ultrapure water, the substrate is dipped into an anionic molecular solution. Because the total polymer layer is neutral, the substrate is masked from other positive ions. By simply repeating these two steps, a multi-layer thin film is fabricated. The properties of the multilayer thin films fabricated using this method are determined by both the properties of the molecules in each monolayer and the physical ordering of the

multiple monolayers through the composite multilayer structure. By appropriately choosing the molecules and structure design, the dielectric constant and other properties of thin films, such as thickness, can be easily varied. Further, one or both of the polymer layers can be substituted by charged inorganic nanocluster quantum dots.

Figure 3.2 shows three different models. The multi-segmented geometry shown on the left, in which each segment has a different and distinct property, can be applied to implement a simple waveguide structure consisting of a central core region and surrounded on both top and bottom by ESA-formed cladding layers. Besides, since each bilayer of thin films contribute equally to the whole thickness, the thickness increase linearly with number of bilayers. This is shown in Figure 3.3.

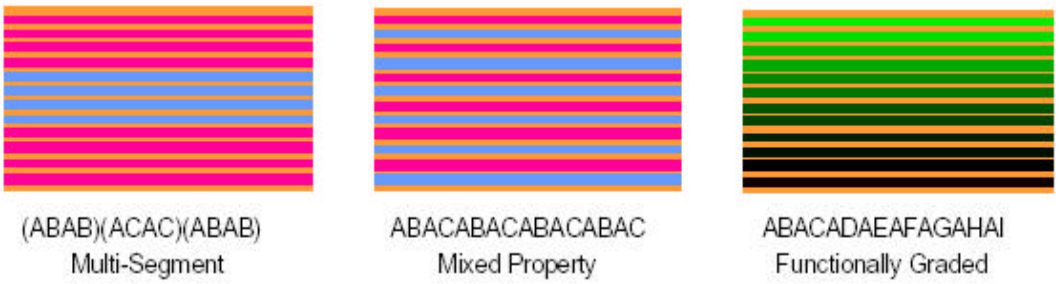

Figure 3.2 Using ESA process, thin-films may be configured to yield segmented (left), mixed (center), and graded (right) property structures.

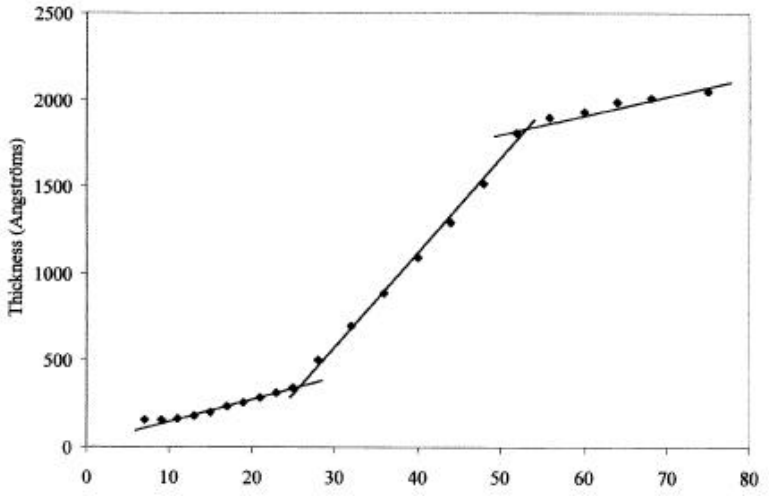

Figure 3.3 Ellipsometrically measured Thickness of $(ZrO_2/PSS)/(Al_2O_3/PSS)/(ZrO_2/PSS)$ multisegment thin film verse number of bilayers.[25]

For mixed molecule coatings, by controlling the percentages of the number of bilayers of each molecule in the total coating, the effective complex dielectric constant can be modified. Alternatively, by gradually changing the relative percent contributions of two or more segments, graded properties may be obtained[27].

3.3 Characterization of ESA formed thin films

Figure 3.4 shows two typical ESA samples and both of their thickness are approximately 40nm. As discussed before, the thickness is proportional to the number of bilayers, as is the optical absorbance.

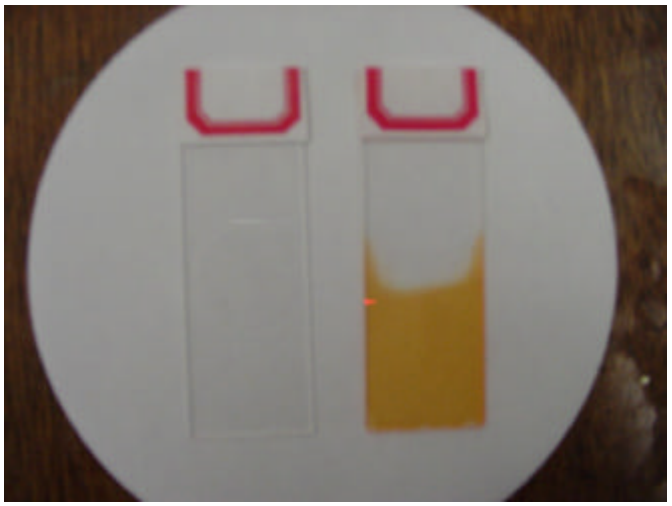

Figure 3.4 Two typical ESA films. Left: PDDA/PSS. Right: PDDA/PS-119.

Figure 3.5 and 3.6 demonstrate material absorbance of a self-assembled PEI/PS-119. An absorbance peak of the PS-119 molecule occurs at around 483nm. Figure 3.6 shows that the absorbance does increase linearly with the number of bilayers as expected by Beer's Law[14]. Using Atom Force Microscope (AFM) to check the surface morphology of the thin films after fabrication, it is obvious that ESA process can provide a very smooth, nano-scaled thin film, and both monolayer species are closely packed and have approximately uniform particle size.

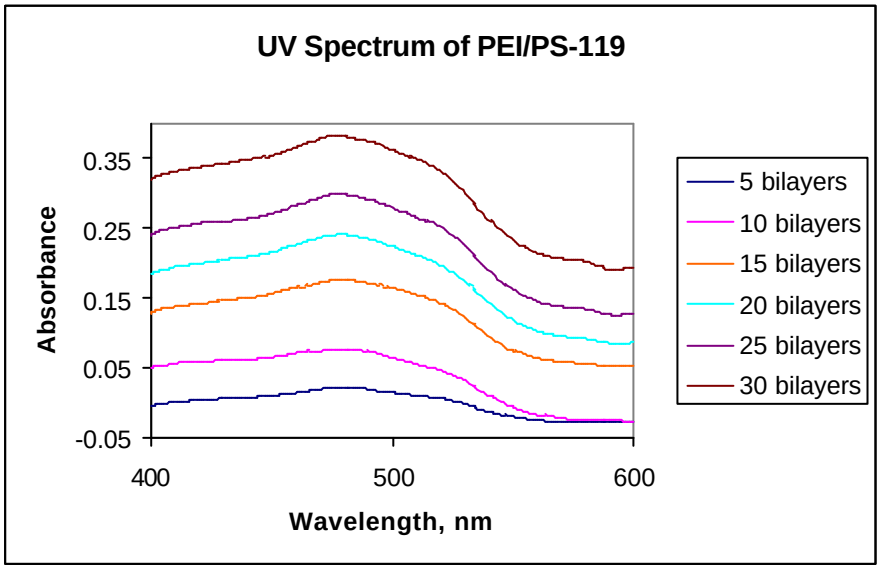

Figure 3.5 UV-Vis spectra of poly (ethylenimine)/PS-119.

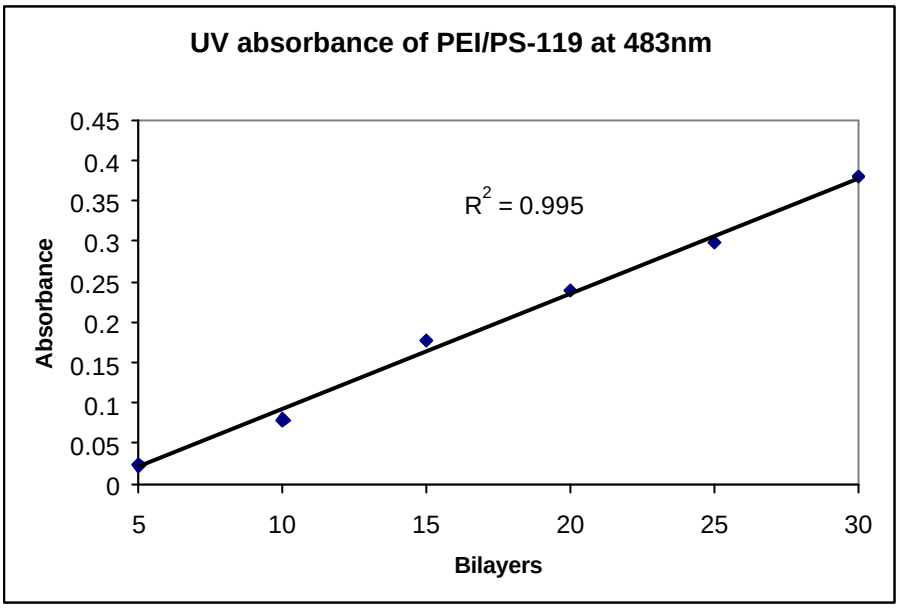

Figure 3.6 UV-Vis absorbance of poly (ethylenimine)/PS-119 at 483 nm.

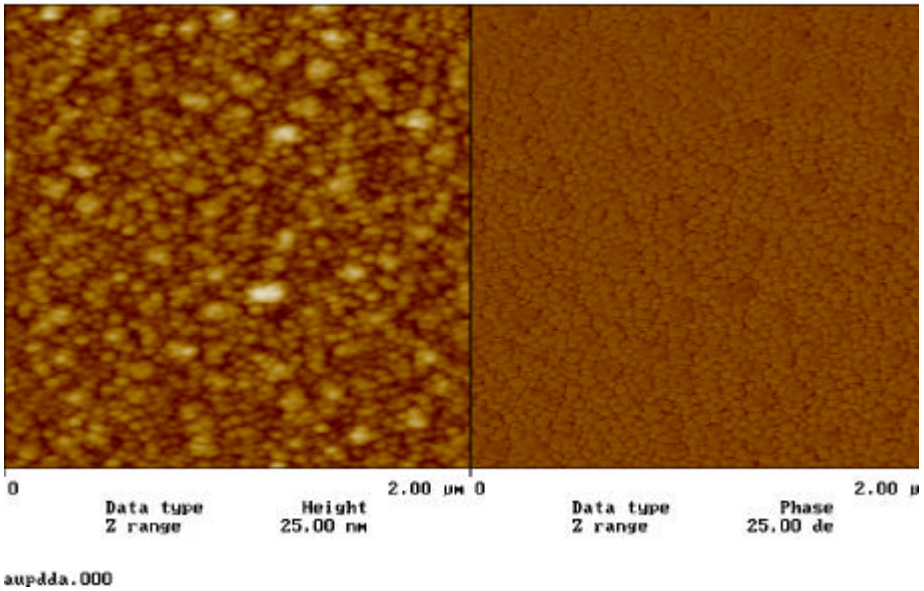

Figure 3.7 AFM Height (left) and Phase (right) images

of PDDA/PMEMA coating on gold-coated glass.

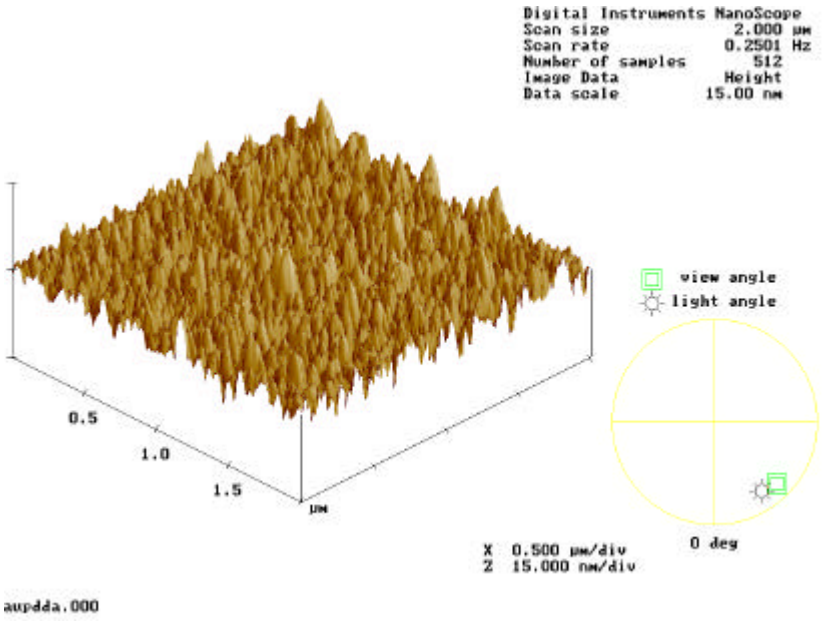

Figure 3.8 AFM View image of PDDA/PMEMA coating on gold-coated glass.

3.4 ESA advantages

Thus, compared to conventional nanofabrication methods, ESA process offers following potential advantanges for making optical thin films[26].

- Easy to fabricate at room temperature and pressure
- Capability for multilayer patterning
- Precision control over thickness and refractive index
- Excellent nanoscale molecular layer uniformity
- Long term stablility since each layer is formed by the molecular autoarrangment and molecules are in an stable equilibrium
- Low cost manufacturing with automated dipping systems
- Friendly environment involving no volatile organic compounds and consuming negligible electrical power
- Independent of substrate size and topology

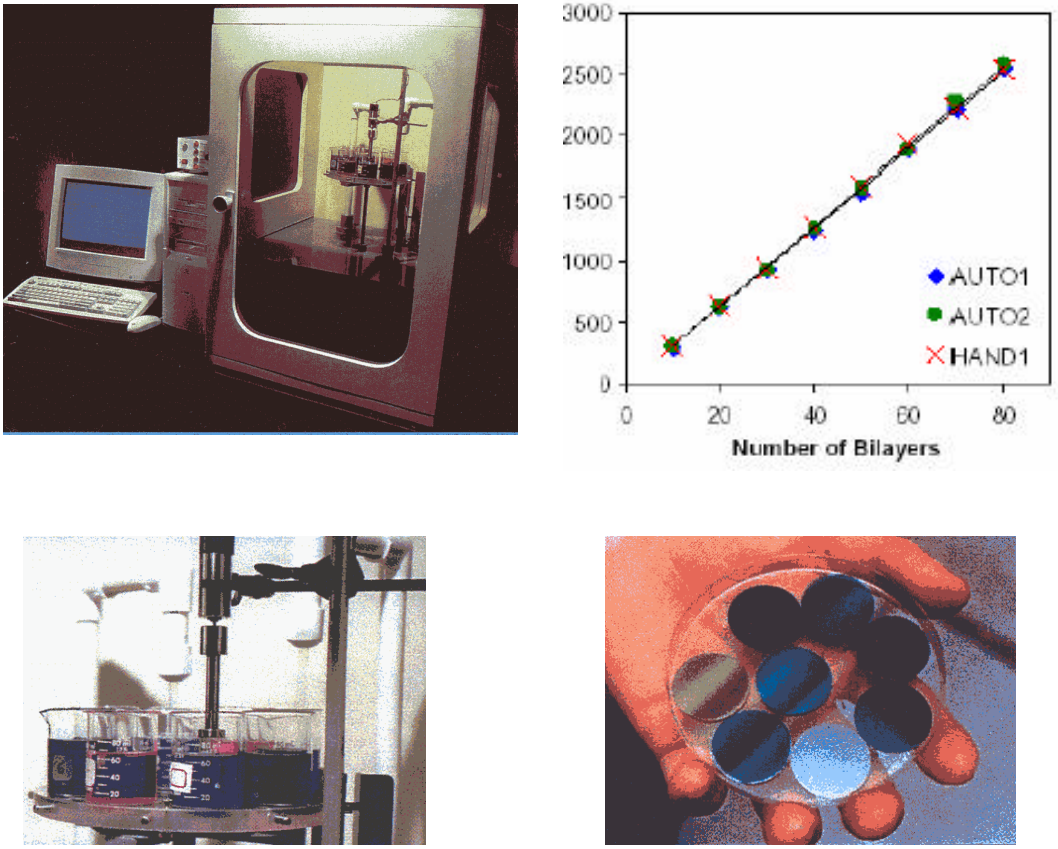

Figure 3.9 shows an automated dipping machine used to fabricate multiple ESA sample materials. Up left: Automated dipping machine, Right: Linearity of machine dipped sample VS. Hand made samples. Bottom left: dipping processing, right: dipping samples

Chapter IV Test preparation

4.1 Introduction

As previously stated, the primary scope of this thesis is to use the electrostatic self-assembled monolayer synthesis process to fabricate a Fabry-Perot cavity. The proposed sensing scheme is based on the refractive index change with relative humidity of such a film applied to the end of an optical fiber. That is, the change in reflected optical power indicates certain humidity. To achieve this, specific chemical-sensitive coating materials were used to form nanometer-scale Fabry-Perot interferometric cavities[28]. In this chapter, a description about experiment setup and the fabrication procedure of the ESA-based fiber optical humidity sensor is presented. As indicated, we also designed optoelectronic breadboard circuits to support the humidity sensor instrumentation.

4.2 Thin-film Design

In this work, the ESA process is used to fabricate simple alternating multilayer thin films of polymers and nanoclusters, of the design ABAB as shown in Fig 3.2. In Figure 4.1, the sensing scheme is shown, where the refractive index of material H is higher than the refractive index for material L. By alternatively dipping the fiber ends into water solutions of these materials, a multisegment sensor coating shown in part b of Figure 4.2 was formed[25]. The materials chosen to form the multilayered thin films need to provide an optical modulation response to humidity.

Figure 4.1 compares the reflected power of coated and uncoated optical fibers, and it is obvious that the ESA-based thin film greatly improves the humidity sensing ability of the optical fiber.

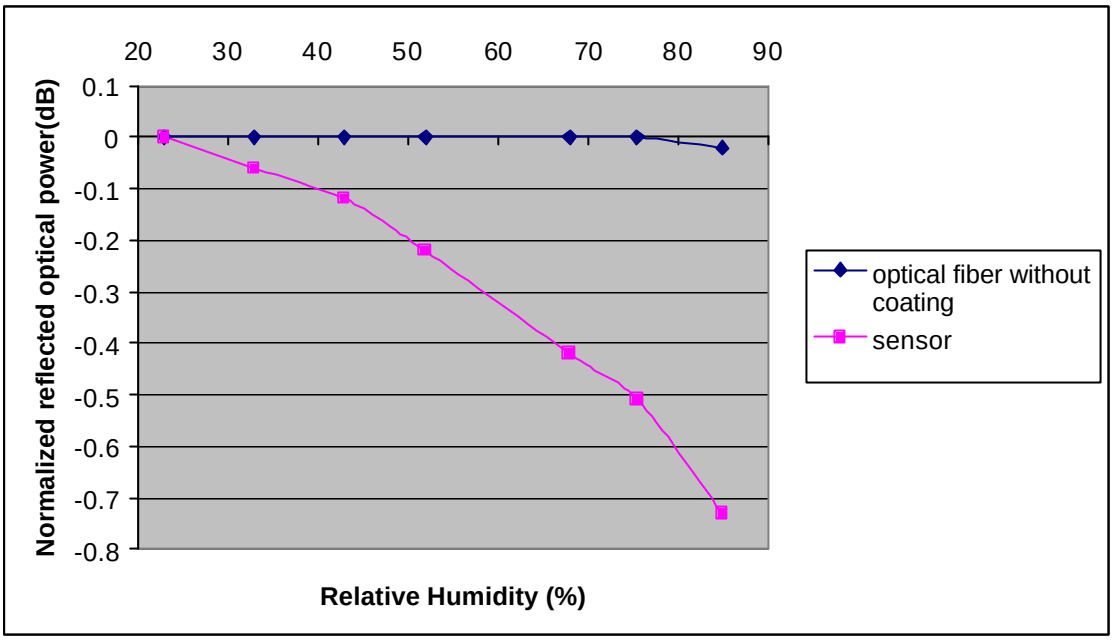

Figure. 4.1 Performance of fiber optic relative humidity sensor fabricated with ESA process.[15]

In the HLHLH nano-Fabry-Perot structure, a solution of poly (diallyldimethyl ammonium chloride)(PDDA) was used to form the cationic electrolyte and solutions of poly (sodium 4-styrene-sulfonate) salt (PSS) and Poly S-119 (polymeric dye, PS119) were used to form the anionic electrolyte. The material H is obtained by the combination $[PDDA^{+}/PS119]_{n}$, where n indicates the number of bilayers of PDDA and PS119 deposited.The material L is fabricated by deposition of $[PDDA^{+}/ PSS]_{n}$.

The final structure has the form: $[PDDA^{+}/ S119]_{28}/[PDDA^{+}/ PSS]_{41}/[PDDA^{+}/S119]_{24}/[PDDA^{+}/ PSS]_{38}/[PDDA^{+}/S119]_{19}$. All polymers used here are commercially available and were purchased from Aldrich. Fig. 4.3 show the molecular structure of these three polymers[23,24,29-31].

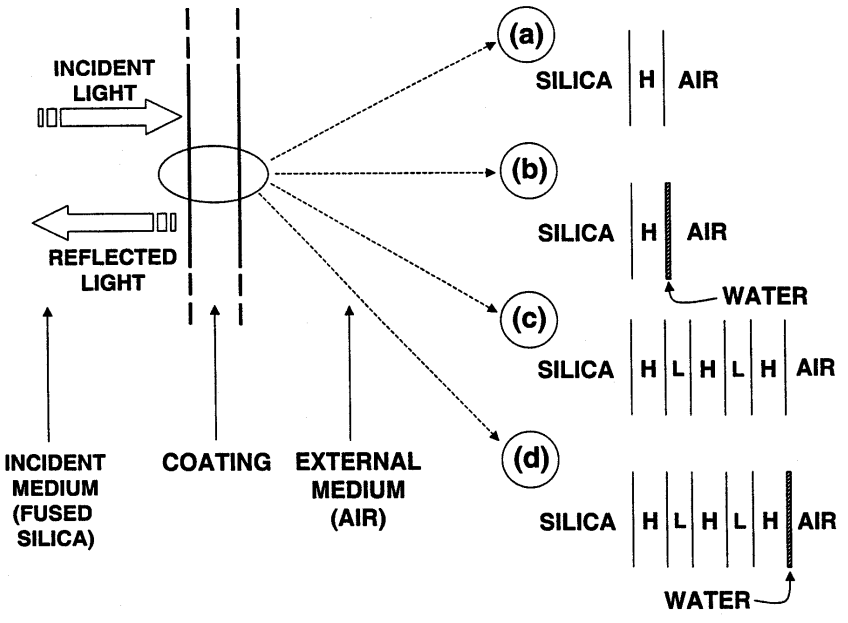

(a)

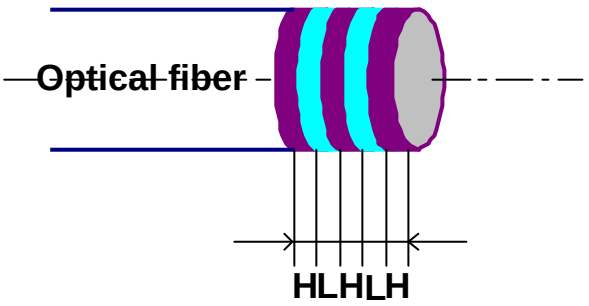

(b)

Figure 4.2 Design (a) of multilayered humidity sensor coating on the end of an optical fiber (b). This design allows direct computer analysis of reflection characteristics using TFCalc™, a commercial optical thin film design software program. [19,20]

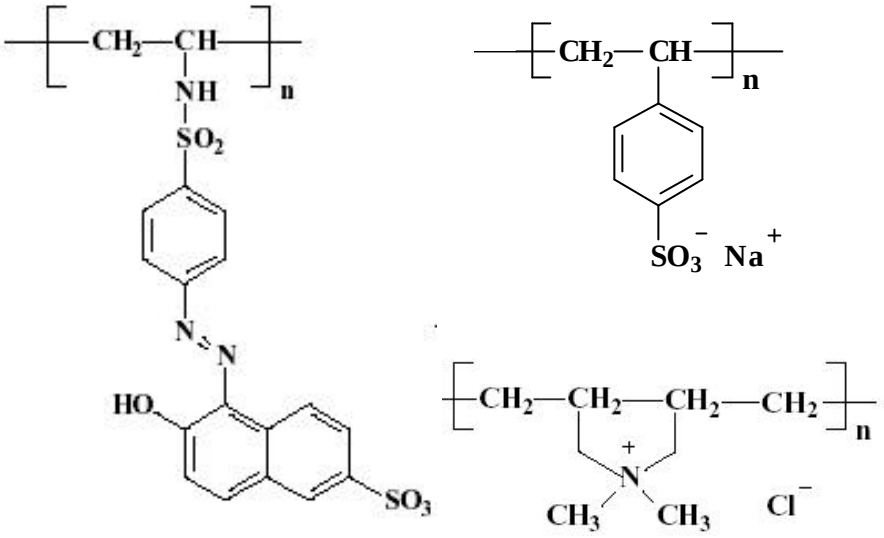

Figure 4.3: Left-PS-119 molecular structure. Up Right-PSS molecular structure.

Up-Right-PDDA molecular structure.

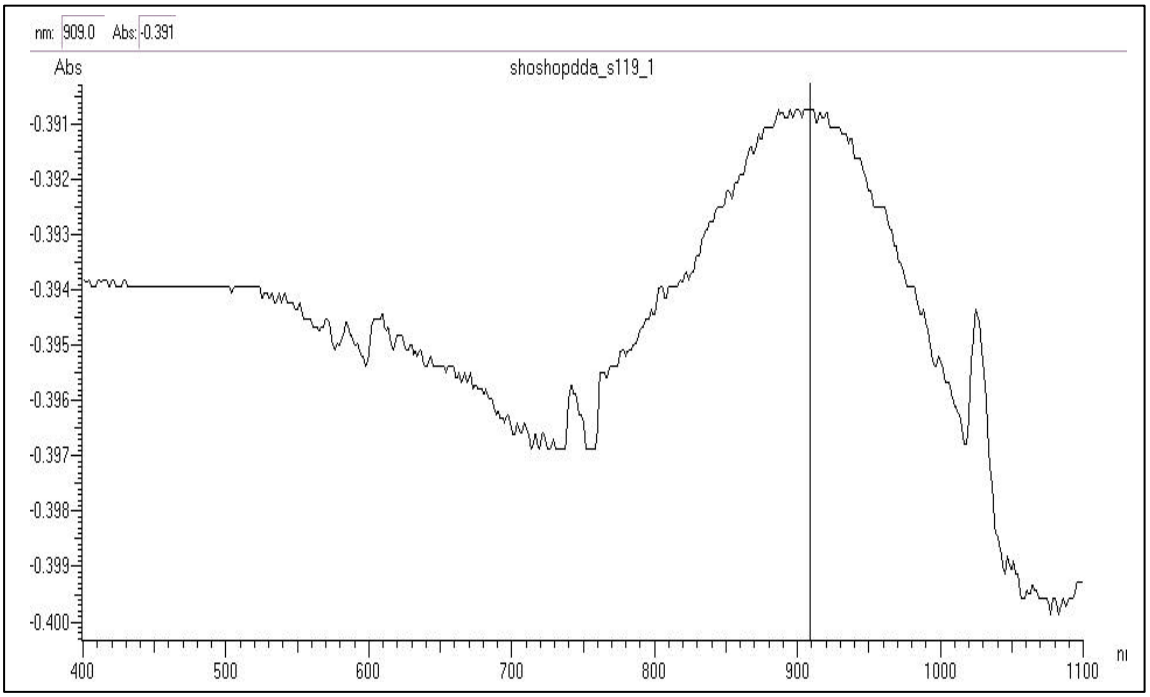

Figure 4.4 UV Spectrum of PDDA/PS-119.

4.3 Making the filter element on the end of the fiber

Fig. 4.5 shows the basic elements for making a thin film coating at the end of the optical fiber. Here, two kinds of fiber were used: a standard step index multimode fiber which has a core diameter of 62.5 microns and a cladding diameter of 125 microns; and a standard step index singlemode fiber which has a core diameter of 9 microns and same cladding diameter as the other multimode fiber. Picture (a) shows the required equipment to cleave and clean the end of optical fiber. (b) is the solution we prepared for coating. Ultra pure water which is obligatory for ESA processing is shown in picture (c).By alternately dipping the fiber end into cationic and anionic molecular solutions (pictures (d) and (e)), a humidity sensitive thin film coating is deposited to the end of the fiber. Picture (f) and (g) show the outlook of completed sensor head. Under microscope, a humidity sensor fiber end with nano-structured coating is shown in picture (h).

(a)

(b)

(c)

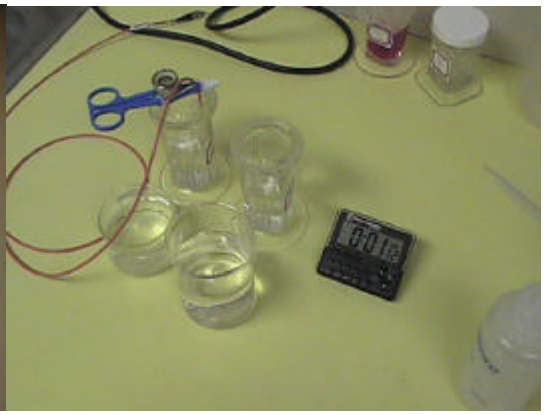

(d)

(e)

(f)

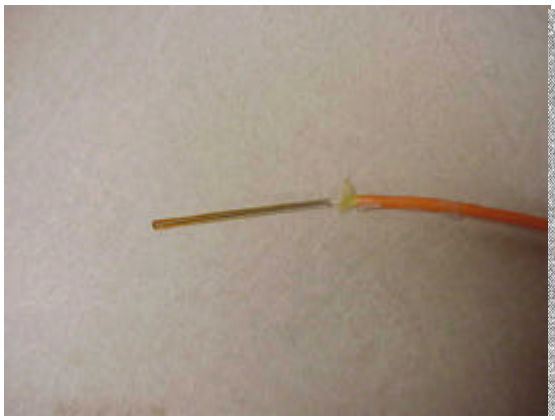

(g)

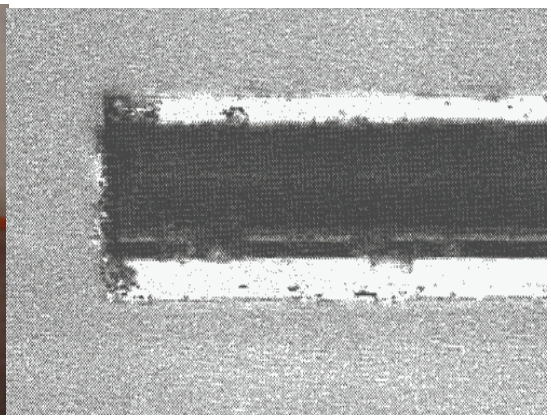

(h)

Figure 4.5 Making a humidity fiber sensor head.

4.4 Experiment Set up

Figure 4.6 shows a simplified schematic of the sensor system, and Figure 4.7 shows the laboratrory test set-up corresponding to this schematic. An 850nm pigtailed LED, a standard 3dB fused biconical tapered coupler and an InGaAs PIN diode detector were assembled. As shown in Fig. 4.6, output light from the LED source is split by the coupler and feeds both the sensor element and a reference detector. The light reflected from the sensor element end face travels back through the coupler and is detected by the signal detector.

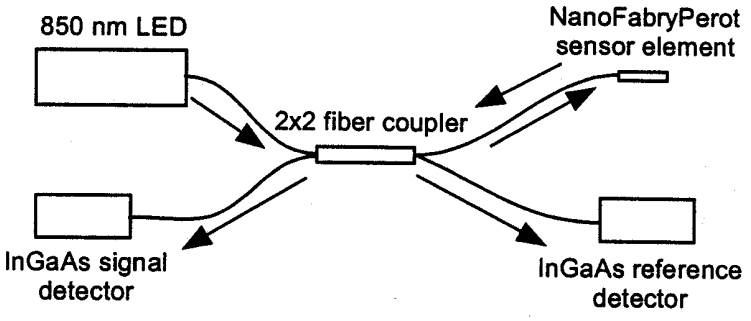

Figure 4.6 Experimental Laboratory set up.

Figure 4.7 Laboratory measurement system corresponding to the schematic shown above.

4.5 Circuit design

This section gives additional details about humidity sensor above. Because the humidity sensor could be apply to flow detection, which will be mentioned in the next chapter, detecting circuit demands high S/N ratio to eliminate any possible effects due to spurious intensity variations on the signal output. In practice, a shield box could be applied to further improve S/N ratio. The circuit below is a simple model of our design, and it's basic function is to convert the optic signal to electric signal using InGaAs detector, then use two level amplifier to increase the signal, which therefore can be observed on a oscilloscope.

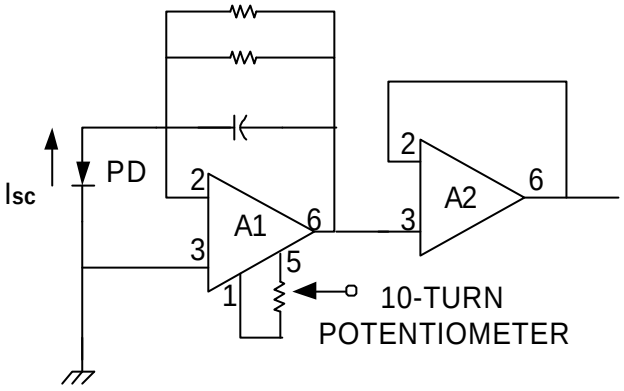

Figure. 4.8 Prototype Low-Cost ESA Sensor Electronics
(where A1 is AD549 and A2 is OP07).

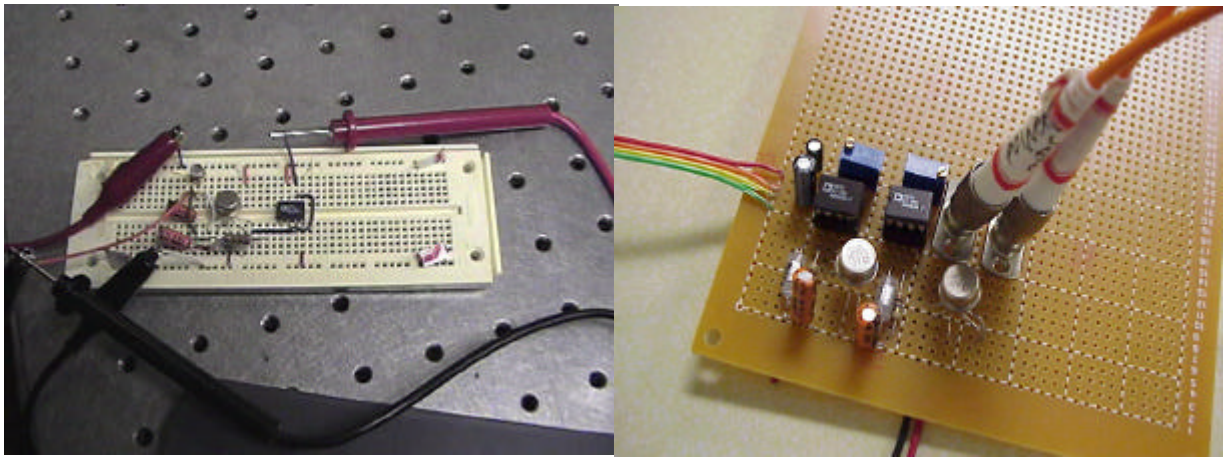

Figure. 4.9 Left: Breadboard Circuit Design. Right: Detecting Circuits (Two Channels) used for air flow rate detection.

Chapter V Testing the sensor

5.1 Introduction

Using the ESA method, we fabricated a Fabry-perot cavity-based optical fiber-based humidity sensor. In this chapter we summarizes the results of the experiments described in the previous chapter. This chapter is organized as follows: first, we demonstrate the performance of fiber-based humidity sensor. Second, two applications of our humidity sensor are described, including human breathing monitoring and air flow rate measurement. At last, conclusions about ESA based fiber optical sensors are given.

5.2 Testing of humidity sensors

It is necessary to recall that the sensing scheme here is to measure the reflected power from the front and back surfaces of the film, which is coated at the end of an optical fiber. The fabrication process has been discussed in Chapters 3 and 4. And as explained in chapter 2, the coating film at the end of the fiber functions as a Fabry-perot cavity, and this hypothesis is clearly demonstrated by a graph below.

Figure 5.1 shows the reflected optical power from a $[PDDA^{+}/PS\text{-}119^{-}]_n$ and $[PDDA^{+}/PSS^{-}]_n$ thick film coating for multimode fiber (MMF), where "n" indicates the number of total assembled bilayers, and again, a bilayer is defined as the combination of one cationic monolayer and one anionic monolayer. From Figure 5.1, it is observed that the first peak in the back reflection interference signal appears for a layer thickness of about 30 bilayers for material $[PDDA^{+}/PS\text{-}119^{-}]_n$, and this thickness corresponds to a quarter of the wavelength of the 850nm source. For $[PDDA^{+}/PSS^{-}]_n$ coating, the first peak in Figure 5.1 occurs approximately at 30 bilayers too, which is also equivalent to a quarter optical wavelength thickness coating of $[PDDA^{+}/PSS^{-}]_n$.

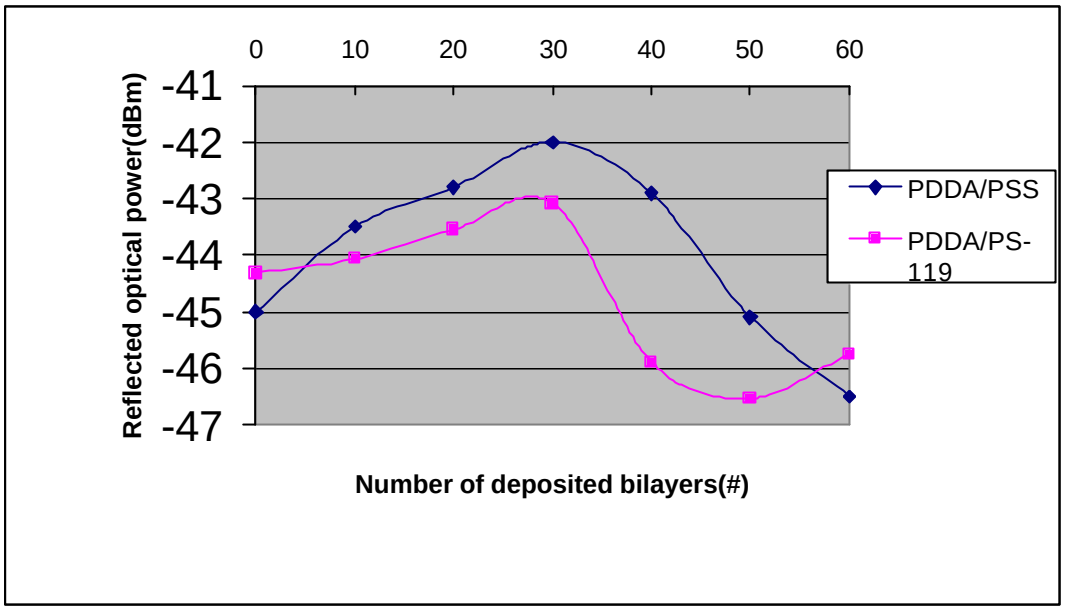

Figure 5.1 Reflected Optical Power Versus number of bilayers of $[PDDA^{+}/S\text{-}119^{-}]_n$ and $[PDDA^{+}/PSS^{-}]_n$ in an Intrinsic Low-finesse Fabry-Perot configuration(MMF).

Figure 5.2 shows the reflected optical power from a $[PDDA^{+}/PS\text{-}119^{-}]_n$ thick film coating for singlemode fiber, and it is obvious that SMF has similar response as MMF, while the reflected optical power is much less than the MMF. The reason for it is the light source we are using is LED, therefore the light coupled into SMF is much smaller than the light into MMF.

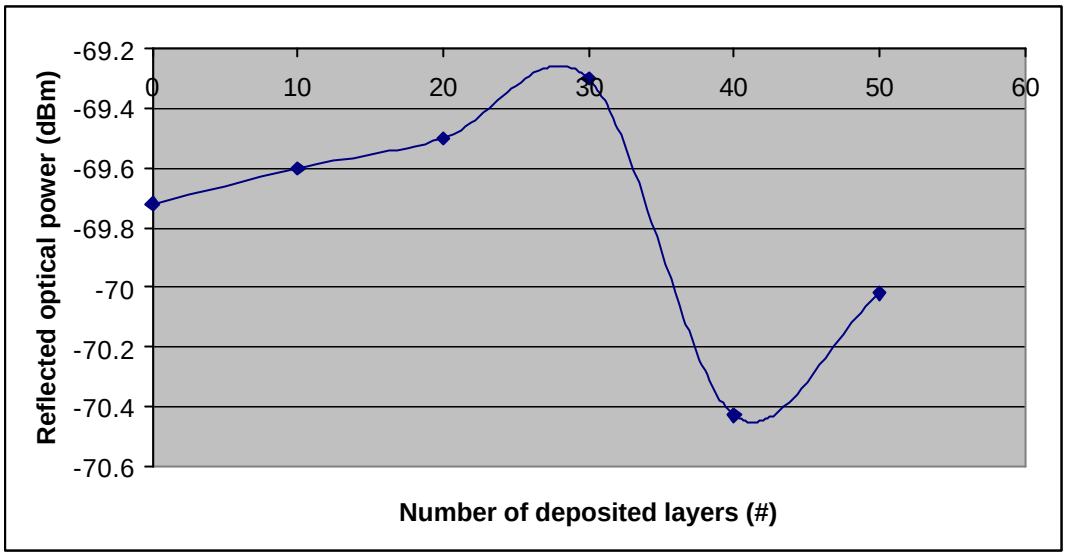

Figure 5.2 Reflected Optical Power Versus number of bilayers of $[PDDA^{+}/S\text{-}119^{-}]_n$ in an Intrinsic Low-finesse Fabry-Perot configuration (SMF).

Based on these initial results, intrinsic Fabry-Perot sensor responses for different numbers of bilayers of $[PDDA^{+}/PS\text{-}119^{-}]_n$ on the ends of optical fibers were determined versus relative humidity. The humidity was controlled by forming different known chemical solutions in closed containers to create different relative humidity conditions due to the partial pressure of these solutions. Since the humidity provider by the chemicals are not contact with outer environment, the humidity measured in this thesis is actually relative humidity. These materials are shown in Table 5.1.

SALT	%HR ($20^{o}C$)
LiCl	11.3
CH_3COOK	23
$MgCl_2$	33
K_2CO_3	43
$Mg(NO_3)_2$	52
$CuCl_2$	68
NaCl	75.5
KCl	85

Table 5.1 Relative humidity of some chemical solutions in the air (under room temperature). [32]

Data shown in Fig. 5.3 corresponds to 30 bilayers and 40 bilayers of PDDA and PS-119, labeled 1 and 2, respectively, and polynomial fits of these two curves are also presented in the same graph. This representative data shows generic sensor response, and it corresponds to the Figure 5.1 that because reflected signal reaches its first peak around 30 bilayers, the output level shown in Figure 5.3 of 30 bilayers is higher than 40 bilayers.

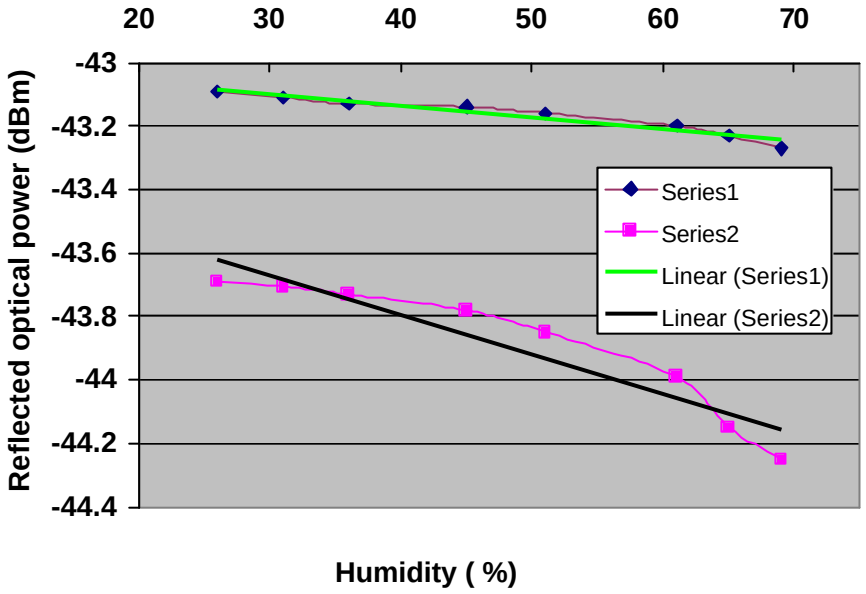

Figure 5. 3 Sensor output vs. relative humidity and their Corresponding polynomial fits.

From the generic, representative information shown in Figure 5.1- 5.3, it may be concluded that by varying the thickness of the Fabry-Perot sensor layer, the sensitivity to humidity may be changed for both MMF and SMF. However, thicker coatings respond more slowly to changes in humidity due to molecular diffusion time effects.

To extend this ananlysis and demonstration, PS-119 were replaced by Poly (sodium 4-styrene-sulfonate) salt (PSS) to fabricate a thin film again. And corresponding humidity

sensor data shown in Fig. 5.4 corresponds to 10, 40, 60 and 70 bilayers of $[PDDA^{+}/PSS^{-}]_{n,}$ labeled 1 to 4, respectively. Fig. 5.5 shows this raw data fit to polynomial curves.

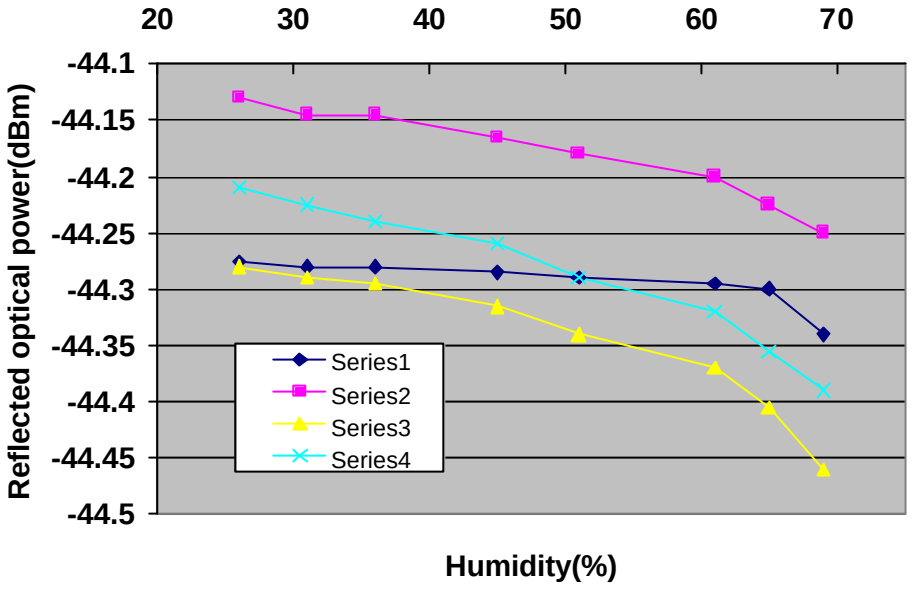

Figure 5.4 Sensor Output Versus Relative Humidity ($[PDDA^{+}/PSS^{-}]_{n}$).

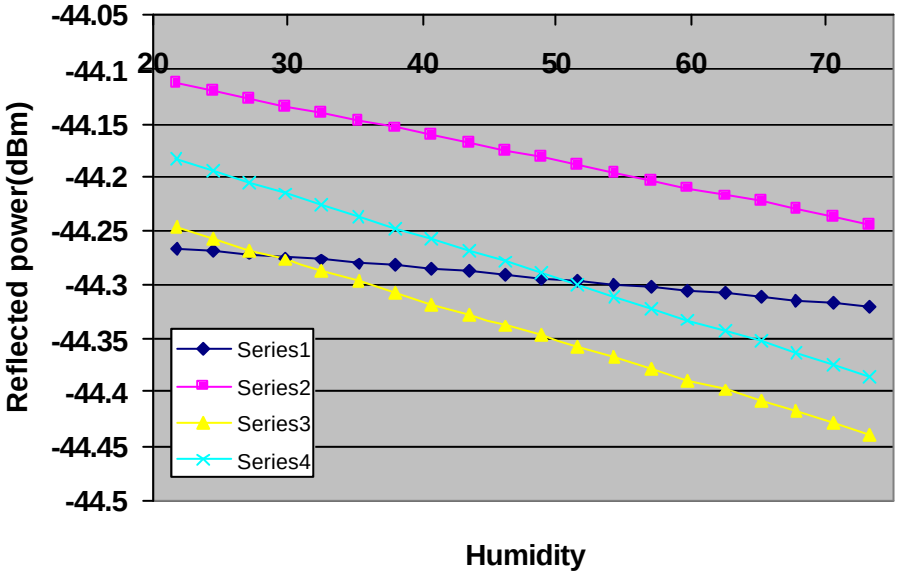

Figure 5.5 Polynomial fit of raw experimental data corresponding to Figure 5.4.

5.3 Grating structured nano-Fabry-Perot sensor

Recall from Figure 4.2 in section 4.2, we designed a HLHLH nano-Fabry-Perot fiber-based humidity sensor. The material H is obtained by the combination $[PDDA^{+}/PS119^{-}]_{n}$, and $[PDDA^{+}/PSS^{-}]_{n}$ functioned as material L. The complete structure has the form: $[PDDA^{+}/S119^{-}]_{28}/[PDDA^{+}/PSS^{-}]_{41}/[PDDA^{+}/S119^{-}]_{24}/[PDDA^{+}/PSS^{-}]_{38}/[PDDA^{+}/S119^{-}]_{19}$. Our hypothesis is that multiple cavity layers should produce different output responses. In this section, the sensor responses for different numbers of grating periods at the end of sensor head were given versus relative humidity. By trading off cavity layer number and response output, an optimal balance between required manufacturing time and sensor performance could be achieved.

Using the same way to control humidity, Figures 5.6-5.10 shows six different sensor geometries, in which series from 1 to 6 represent different grating structures, namely and in order: a quarter wavelength thickness coating of material H; and gratings HL, HLH, HLHL, HLHLH and HLHLHL, respectively.

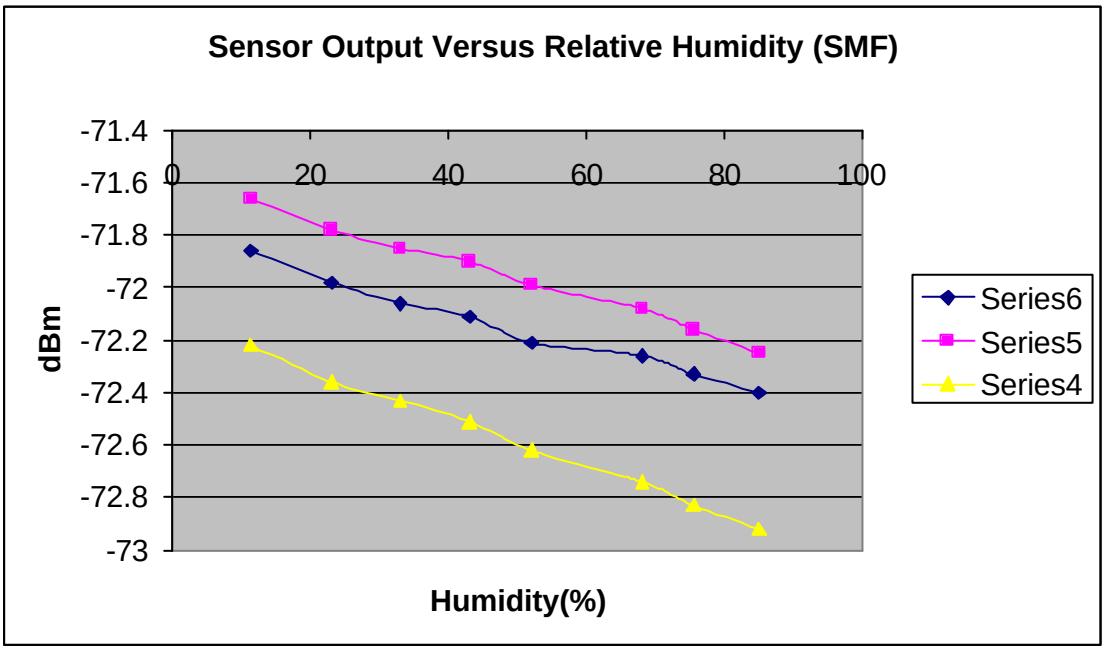

Fig. 5.6 Sensor Output Versus Relative Humidity (SMF).

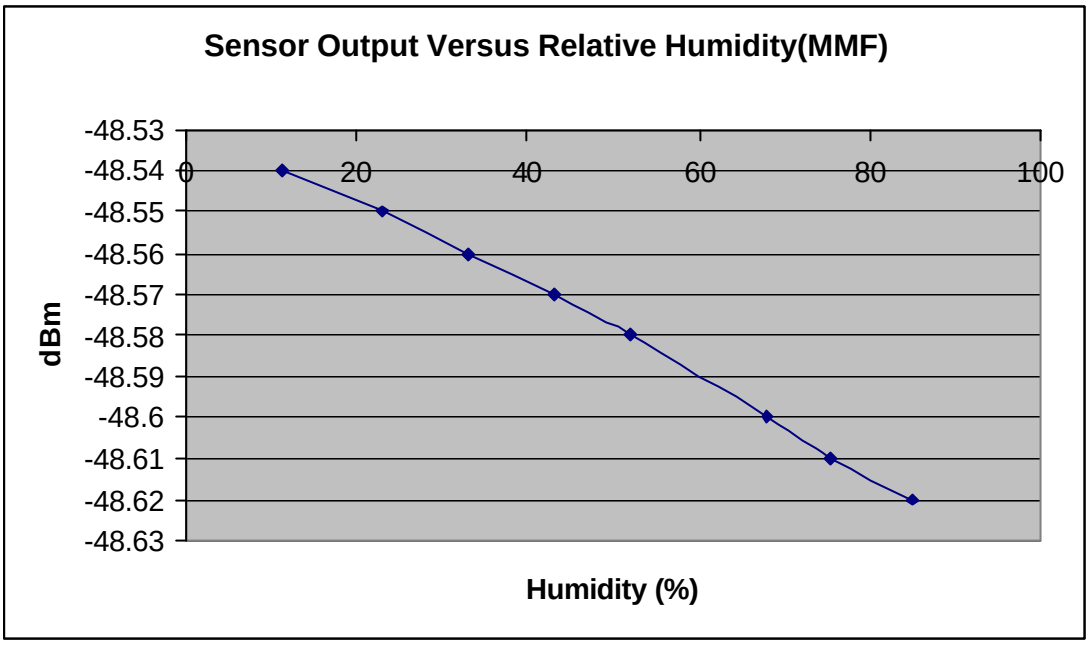

Fig. 5.7 Sensor Output Versus Relative Humidity (MMF),

which corresponds to the series 6.

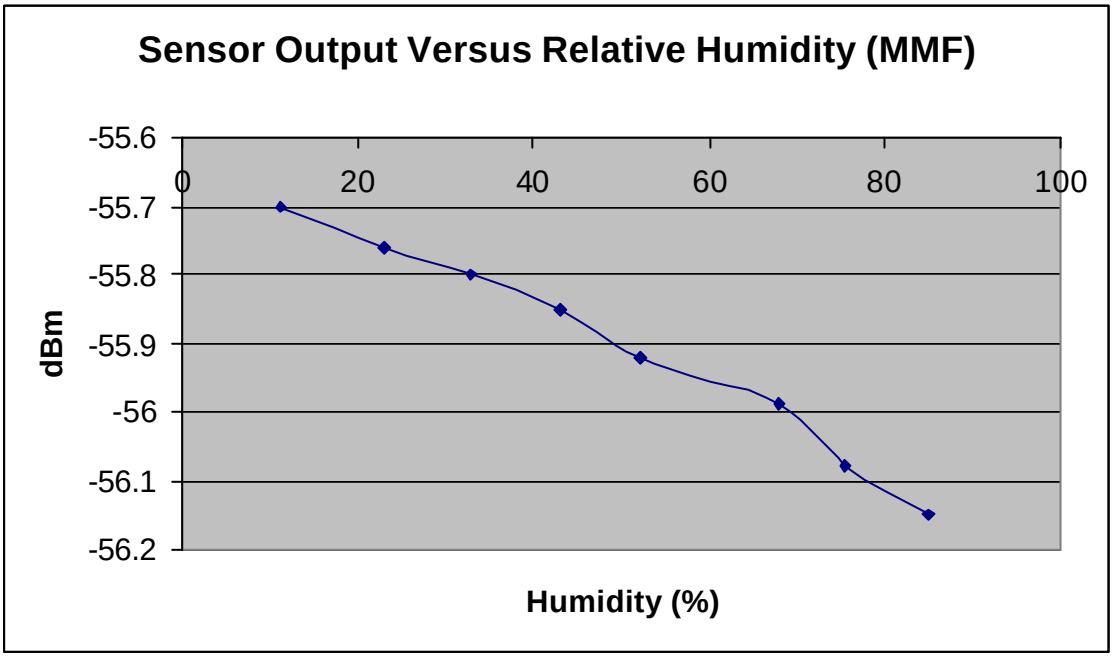

Fig. 5.8 Sensor Output Versus Relative Humidity (MMF),

which corresponds to the series 5.

Using the circuit designed in chapter 4, the output shown in mV in Figures 5.9 and 5.10 was obtained, and it is shown that the data has an increased amplitude with an increase of humidity. As demonstrated, the nano-grating structure does improve the sensitivity of optical fiber humidity sensor.

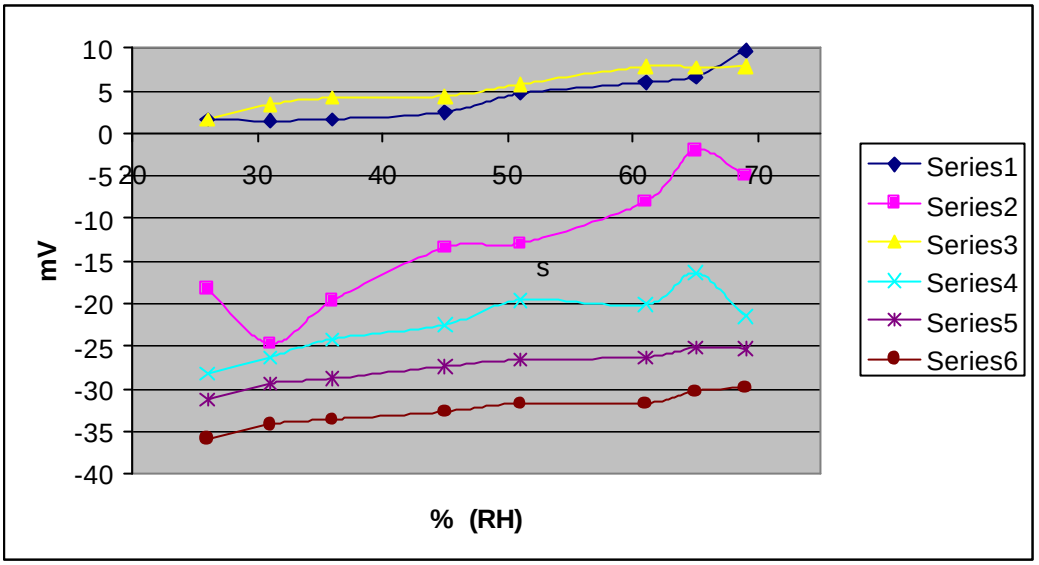

Figure 5.9 Reflected optical powers versus relative humidity.

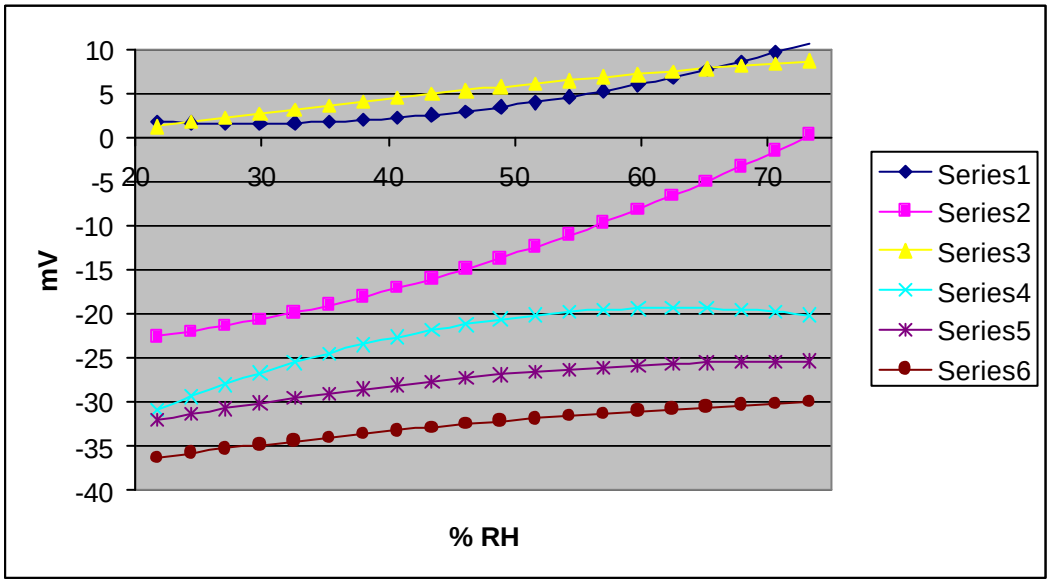

Figure 5.10 Polynomial fit of raw experimental data shown in Figure 5.9.

5.4 Human breath monitoring

Further, we have investigated the frequency response of sensors and have measured a 10% to 90% signal rise time. Experimental results prove that the films deposited by the ESA method on optical fibers have fast response time with an order of 10s of milliseconds or less. That is to say, such humidity sensor could lead to improvement of health care, since similar response time of commercial humidity sensors is on the order of several seconds[34]. Figure 5.11 demonstrates the ability of our humidity sensor to on-line monitoring human breathing. (Using software 'Starwave' to withdraw data from oscilloscope, than redraw it by software 'Origin')

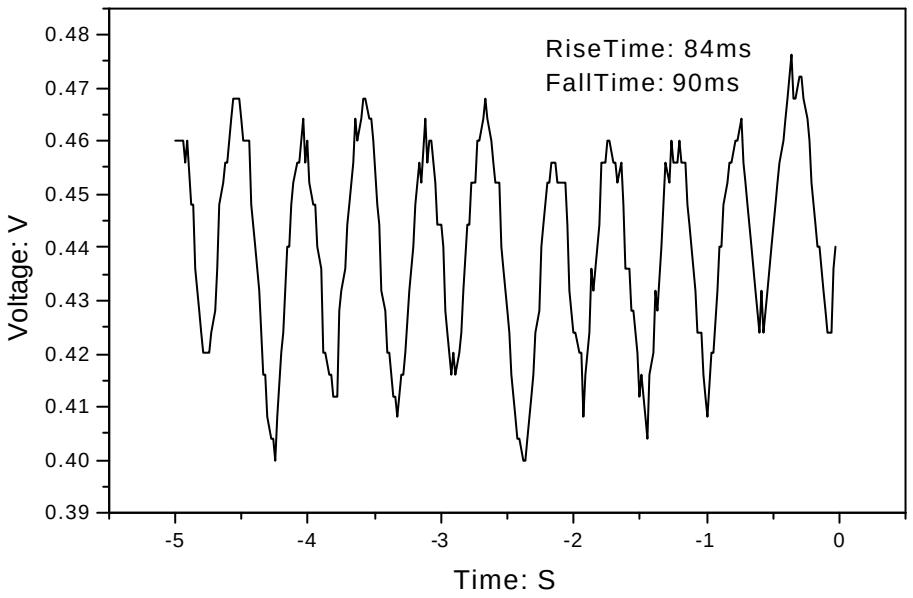

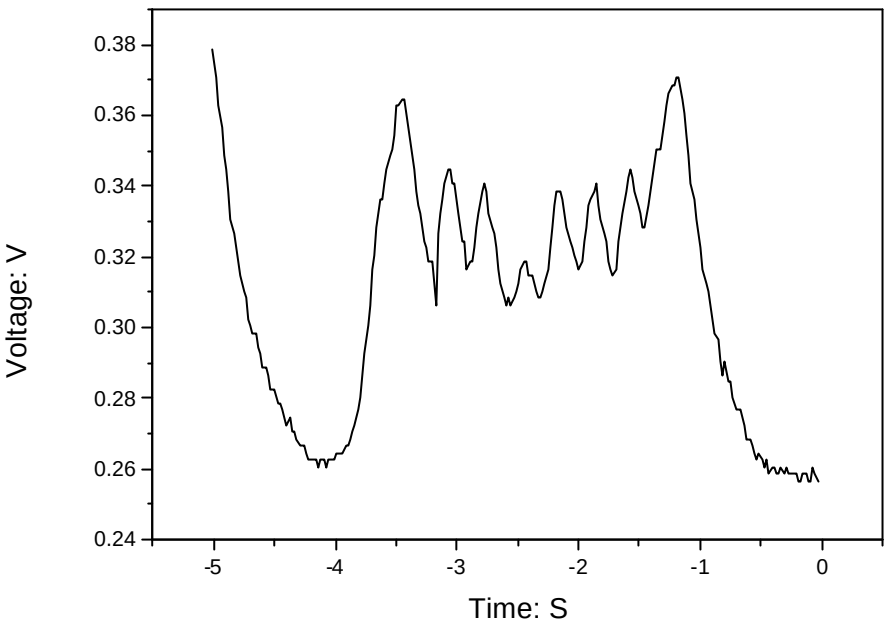

Figure 5.11 Sensor system response to simulated human breathing

Top: Rapid Breathing. Bottom: irregular Breathing. [35]

The significance of this human breathing monitoring is that our humidity sensor is physically small and could be used as a real time instrument. Figure 5.12 shows oscilloscope traces, corresponding to the humidity changes associated with repetitive human breath simulated by a respiration simulator.

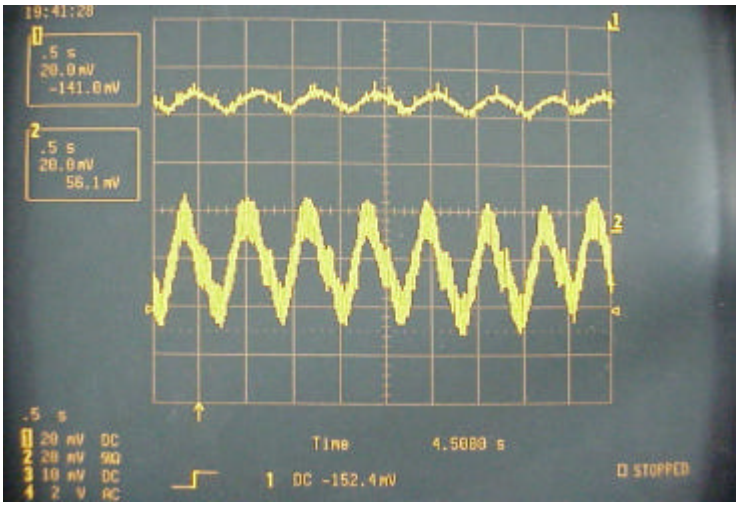

Figure 5.12 Human breath tracking use ESA humidity sensor and respiration simulator.

5.5 Air flow sensor

Because of the fast response, such humidity sensors could also be used to characterize of dynamic humidity-related processes such as humid airflow rate. By knowing air flow rate, the cross-sectional dimension airway, and the relatively humidity of the flowing air, quantitative measurement of water vapor transport may be obtained, and this result is important to the understanding and diagnosis of respiratory problems and diseases.

To measure the flow rate of humid air associated with human breathing, two of the ESA-formed optical fiber sensors were arranged as shown in Fig. 5.13, in such a way that the sensor ends of the fibers were physically separated along the vector direction of the air flow. The simple fiber sensor multiplexing network diagramed was assembled, as shown in figure 5.14. If the two sensor heads are spaced apart by a distance d, and if the time separation of two detected breath signatures is Δt as shown in figure 5.15, then the air flow speed is given simply as

$$speed = \frac{d}{\Delta t}.$$

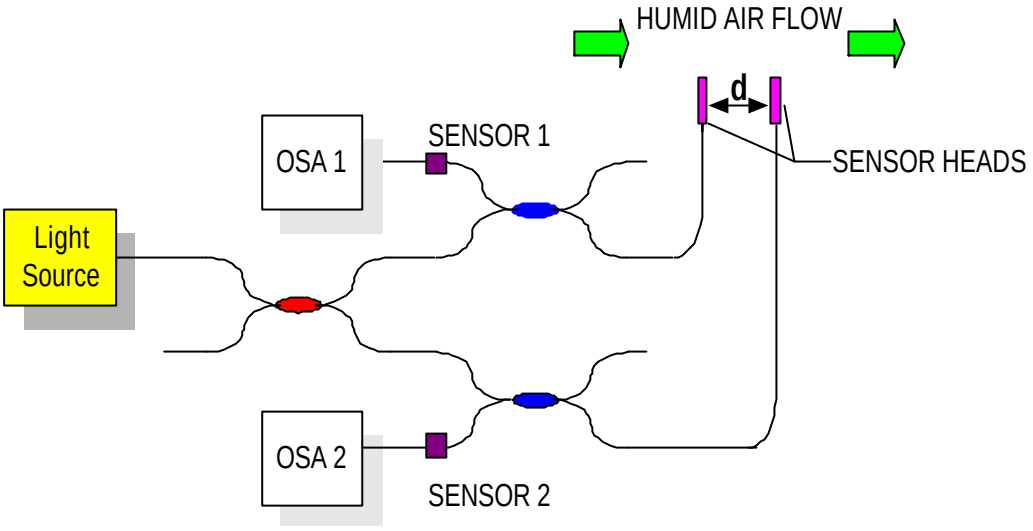

Figure 5.13 Two ESA Humidity Sensor Multiplexing Network for Measurement of Air Flow Rate.

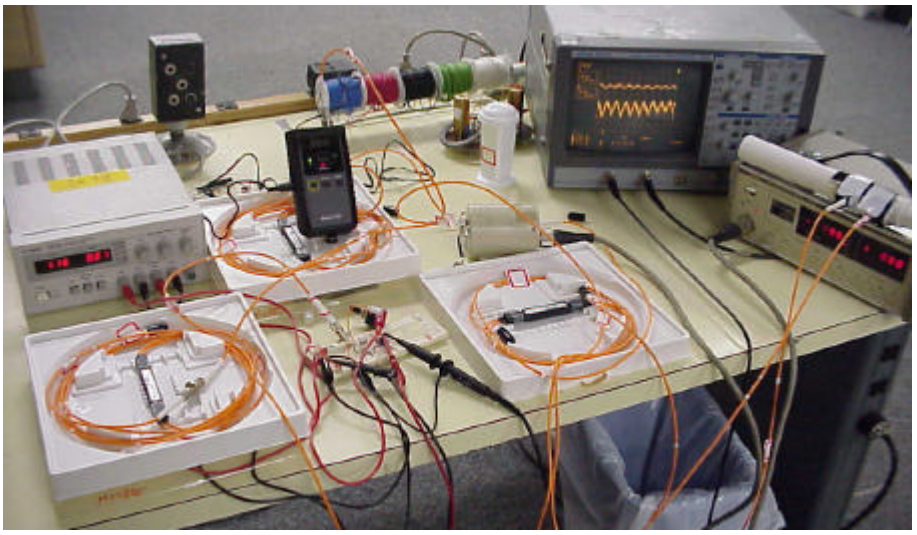

Figure 5.14 Laboratory set-up for Measurement of Air Flow Speed.

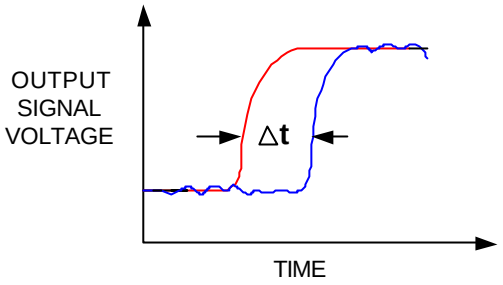

Figure 5.15 Determination of Air Flow Rate From Two Sensor Output Signals.

Figure 5.16 shows an early laboratory prototype, literally a tube with two holes to accommodate the mounting of two sensor probes, that may be connected directly with a respiration simulator.

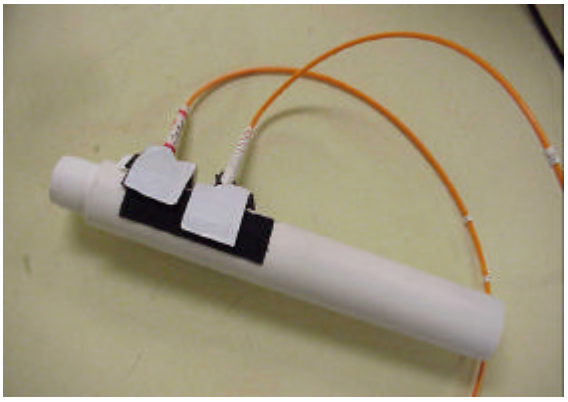

Figure 5.16 Prototype for measurement of air flow.

5.6 Conclusion

In this chapter, we tested our ESA based humidity sensor, achieving a fast response time, which is on the order of microseconds. Near real-time response allows measurement of time-dynamic processes, including human airway and pulmonary diagnostics. This will lead to faster and better diagnostics, more rapid and scientific treatment, and improved health care. Furthermore, using two ESA humidity sensor multiplexing network, air flow rate and water volume transport may be determined.

Chapter VI Suggestion for future work

6.1 Alternate sensor head geometries

Through future work, we can investigate possible alternative methods for fabrication of the sensor heads, as shown in Figure 6.1. Both of these designs may allow greater signal modulation due to increased sensor area, while potentially eliminating the need for the fiber coupler in the lab setup, hence reducing the sensor system manufacturing and sales costs.

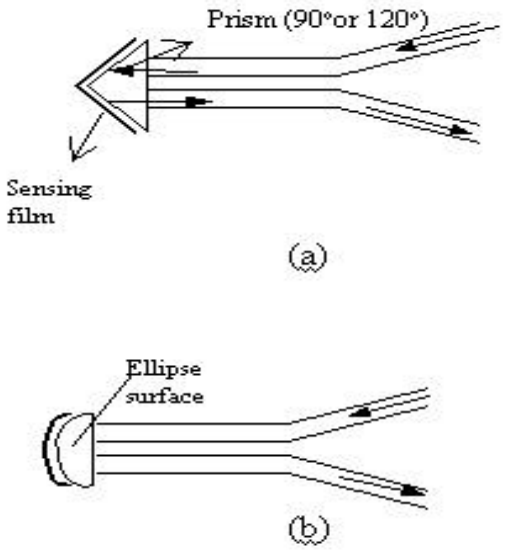

Figure 6.1 Alternate sensor head geometries.

6.2 New material for humidity sensing

Organic polymeric materials have been widely studied for moisture detection, including PDDA, Poly (2-acrylamido-2-methylpropane sulfonate) and others. Such polymers can absorb water from the environment and undergo large changes of their properties before and after adsorbing water. In future work, we suggest to use polyethylenimine (PEI), a

hydrophilic polymer to replace PDDA because –NH groups in its structure can easily form hydrogen bonds with water molecules.

6.3 Possible measures other than humidity

By varying the chemistry of the self-assembled coating on the tip of the fiber sensor element, it has been reported as a means to detect gases, such as oxygen, dichloromethane gas and NH_3. Because of the vast medical market, based on the humidity sensor, we recommend to study gas flow sensors. Although a primary application of such sensor is in the biomedical area, it can also be employed in multiple other markets, such as engine controls in natural gas and diesel motors.

References:

1. D. A. Krohn, "Fiber optic sensors fundamentals and applications," Instrument society of America, -3rd ed, 2000.
2. B. Culshaw and J. Dakin, "Optical fiber sensors components and subsystems," Artech House, Inc. vol. 3, 1996.
3. B.Felton, "Fiber-optic sensors ready to take off?" InTech Magzine, 18 April 2001.
4. E. Udd, "Fiber optic sensors: an introduction for engineers and scientists," New York:Wiley, 1991.
5. J. Fraden, "AIP Handbook of Modern sensors," American Institute of Physics,1993.
6. G. Harsanyi, "Polymer films in sensor applications," Technomic Publishing Company, Inc. 1995.
7. S. Otsuki, K. Adachi and T. Taguchi, "A novel fiber-optic gas-sensing configuration using extremely curved optical fibers and an attempt for optical humidity detection," Sensors and Actuators B 53 (1998), p. 91-96.
8. F. Mitschke, "Fiber-opitc sensor for humidity," Optics letters, vol.14, No. 17.
9. D.C. Bownass, J.S. Barton, and J.D.C Jones, "Detection of high humidity by optical fiber sensing at telecommunications wavelengths," Optics Communications 146 (1998) p.90-94.
10. R.A. Lieberman, " Recent progress in intrinsic fiber-optic chemical sensing II," Sensors and Actuators B, 11 (1993), p. 43-55.
11. G. Gauglitz, G. Brecht, and W. Nahm, "Chemical and Biochemical Sensors based on Interferometry at thinlayers," Sensors and Acutators B, 11(1993), p.21-27.
12. B.D.Gupta, Ratnanjali, " A novel probe for a fiber optic humidity sensor," sensors and Actuators B 80(2001) p. 132-135.
13. C.E.Lee, W.N.Gibler, and et.al, "In-Line Fiber Fabry-Perot Interferometer with High-Reflectance Internal Mirrors," Journal of Lightwave Technology, vol. 10, No. 10, Oct, 1992.
14. M. Born and E. Wolf, "Principles of Optics," -6th ed. Elmsford, NY: Pergamon Press 1980, p.329.

15. F.J.Arregui, Y.Liu, K.Lenahan, C. Holton, I. R. Matias, and R.O. Claus, "Optical fiber humidity sensor formed by the ionic self-assembly monolayer process," Proceedings, Optical Fiber Sensors Conference (OFS-13), Korean, 1999, p.236-239.
16. H.A. Macleod, "Thin-film Optical filters," Techno House, 1989.
17. A.Thelen, "Design of Optical interference coatings," Ed. McGraw-Hill, 1989, p.5-17.
18. K. L. Cooper, "ESA of linear and nonlinear optical thin films," Ph.D dissertation, Vtech, April, 1999.
19. F.J.Arregui, K. L. Cooper, Y. Liu, I. R. Matias, and R.O.Claus, "Optical fiber humidity sensor with a fast response time using the ionic self-assembly method," IEICE Trans. Electron., Vol. E83-C, No.3, Mar 2000.
20. F.J.Arregui, I.R. Matias, Y.Liu, K.L. Cooper and R.O.Claus, "A dichloromethane gas optical fiber sensor fabricated using the electronic self-assembly monolayer method," Proceedings, Optical Fiber Sensors Conference (OFS-14), Italy, Oct 2000, p.400-403.
21. k. Chen, W.B. Caldwell and C.A. Mirkin, 1993 J.Am.Chem. Soc. 115 1193
22. Y.Liu, A. Wang and R.O.Claus, 1997 J.Phys. Chem.B 101 1385
23. Y.Liu, A. Wang and R.O.Claus, "Layer-by-layer electrostatic self assembly of nanoscale Fe_3O_4 particles and polymide precursor on silicon and silica surfaces," Applied Physics Letters. 71 (16), p. 2265-2267, 1997
24. A. Rosidian, Y.Liu and R.O.Claus, " Ionic self-assembly of ultrahard ZrO_2/polymer nanocomposite thin films," Advanced Materials, Vol. 10, p.1087-1091, 1998
25. Y. Liu, A. Rpsidian and etc. "Characterization of electrostatically self-assembled nanocomposite thin films," Smart Mater. Struct. 8(1999) p.100-105.
26. A. Chandran, "Self-Assembled Multilayered Dielectric Spectral Filters," MS. thesis, ECE Dept, VTech, 2001.
27. R.Duncan, "Electro-Opitc properties of self-assembled nonlinear optical polymers," M.S. thesis, ECE Dept, VTech, 2002.

28. F.J.Arregui, I.R.Matias, Y. Liu and R.O. Claus, "Fabrication of micrograting on the ends of standard optical fibers by the electrostatic self-assembly monolayer process," Optics letters, Vol. 26(3), p. 131-133, 2001.

29. F.J. Arregui, Y.Liu, I.R.Matias, K.L.Cooper, and R.O.Claus, "Simultaneous measurement of humidity and temperature by combining a reflective intensity-based optical fiber sensor and a fiber Bragg grating".

30. G. Decher, "Fuzzy nanoassemblies:Toward layered polymeric multicomposites," science, Vol.277, p.1232-1237,1997.

31. K.M.Lenahan, Y.X. Wang, Y.Liu, R.O.Claus, J.R. Heflin and etc, "Novel polymer dyes for nonlinear optical applications using ionic self-assembled monolayer technology," Advanced matericals, Vol. 10 (1998), p.853-855.

32. F.J. Arregui, Y.Liu, I. R. Matias, K.L.Cooper, and R.O.Claus, " Optical Fiber humidity sensor using a nano fabry-perot cavity formed by the ionic self-assembly method," Sensors and Acutators B 3000, 1999.

33. J.M. Meanna Perez, C. Freire, "A poly(ethyleneterepthalate)-based humidity sesor," Sensors and Actuators B 42(1997) p.27-30.

34. K.L.Cooper, Keith Huie, R.O.Claus, etal, "Optical Fiber sensors for breathing diagnostics," SPOE BIOS Conference, San Jose, Jan,2002.

35. Q. Chen, R.O.Claus, and F.J.Arregui, "Optical fiber sensors for breathing diagnostics," Proceedings, Optical Fiber Sensors Conference(OFS-15), Portland, OR, May 2002, p.273-276.

36. D.C. Bownass, J.S. Barton and J.D.C.Jones, "Serially multiplexed point sensor for the detection of high humidity in passive optical networks," Optics letters, Vol.22, No.5, Mar 1, 1997.

37. C.Bariain, I.R. Matias, F.J. Arregui, "Optical fiber humidity sensor based on a tapered fiber coated with agarose gel," sensors and Actuators B 69(2000) p.127-131.

Vita

Qiao Chen was born in Xi'an, China in 1978. She earned a Bachelor of Science degree in Precise Instrument and Design from the University of Tsinghua in June of 2000. In Dec of 2002, she received a Master of Science degree in Electrical Engineering from the Virginia Polytechnic Institute and State University.